TEMPORAL DEVELOPMENT OF 2D AND 3D RIPPLES IN OSCILLATORY FLOW

Kathleen Graham

Submitted in Partial Fulfillment of the Requirements
For the Degree of Bachelor of Science, Honours
Department of Earth Sciences
Dalhousie University, Halifax, Nova Scotia
March 2007

DALHOUSIE UNIVERSITY
Inspiring Minds

Department of Earth Sciences
Halifax, Nova Scotia
Canada B3H 4J1
(902) 494-2358
FAX (902) 494-6889

DATE: May 1, 2007

AUTHOR: Kathleen A. M. Graham

TITLE: Temporal Development of 2D and 3D Ripples in Oscillatory Flow

Degree: BSc honours Convocation: May 2007 Year: 2007

Abstract

Three experiments were performed using a newly developed ripple cart facility, in which the sand bed moves relative to the water, to study the growth and development of 2D and 3D bedforms under oscillatory flow conditions. Conditions of the experiment were designed to simulate wave conditions in a nearshore marine environment, with an oscillation period = 10 s, excursion amplitudes of 50, 60, and 80 cm, and median grain size = 250 μm. Digital photographs of the bed elevation profile were collected at 15 or 30 minute intervals depending on the rate of change of the bedforms. The ripple profiles were analyzed to quantify the temporal development of the ripples. Ripple wavelengths were plotted against time and compared to a logistic growth model. Principal findings of this study are: (1) that the equilibrium ripple wavelengths are comparable to those expected for vortex-type orbital ripples; and (2) that temporal evolution of ripple wavelengths is well-represented by the logistic growth model.

Key words: Logistic growth, ripple growth, ripple profiles, oscillatory flow, equilibrium bedforms, oscillating bed, sediment dynamics

Table of Contents

List of Figures

List of Tables

List of Symbols

a	Amplitude of cart motion (a = 1/2d)
D	$D_{50,}$ median grain size
d	Orbital excursion diameter
λ	Ripple wavelength defined as crest to crest distance
η	Ripple height
n	Number of periods the cart has made
T	Period of cart
t	Time

Acknowledgements

I would like to thank my supervisor, Dr. Alex Hay, for his guidance, encouragement, and support. Richard Cheel was extremely helpful with the Matlab work and the data collection using the ripple cart, and for numerous discussions on all aspects relating to this thesis. Matthew Hatcher provided the diagrams of the cart, as well as help making sure it ran smoothly. Walter Judge wired the camera, laser, and video capture systems, making it possible to obtain images from the cameras. I would also like to thank Stephanie Moore and Owen Brown for their help with the sand size analysis (Stephanie for the sieve calibration, and Owen for the use of the settling column at the Bedford Institute of Oceanography).

1.0: Introduction

1.1: Objectives

The purpose of this thesis is to study the relationships between different factors affecting the development of two-dimensional (2D) and three-dimensional (3D) ripples from a non-rippled state over time under oscillatory flow conditions. These factors include relationships between time, flow parameters (period, T, orbital excursion diameter, d), and sediment parameters (median grain size diameter, D). The ripple characteristics observed are wavelength, λ, and planform geometry. A list of symbols appears on page vi. See Figure 1.1 for definitions of these characteristics as they are used in this study. For the purposes of this experiment, two- dimensional bedforms are those with straight crestlines. Three-dimensional bedforms may have sinuous crestlines or sinuous troughs, or may have truncate crests and crests oriented obliquely to the oscillation axis.

The development of sand ripples is investigated using a newly-developed ripple cart facility in which the sand bed oscillates and the water remains stationary. The results of this study are compared to previous laboratory and field studies of sand ripples produced by oscillatory flow. I expect that the results of this study will give a better understanding of the natural process of ripple formation.

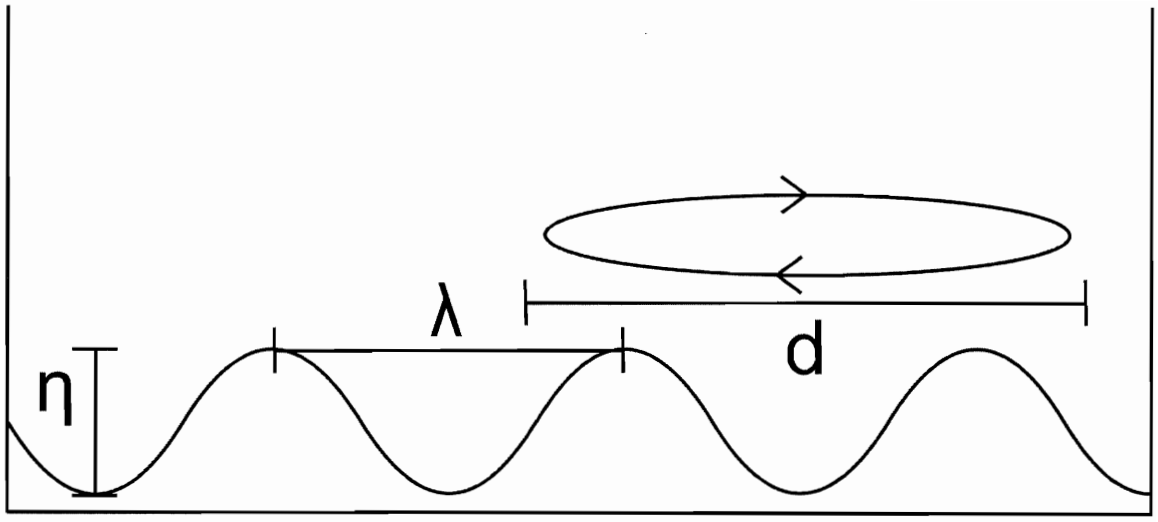

Figure 1.1: Schematic diagram defining ripple wavelength (λ), height (η),and orbital excursion diameter (d), as they are used in this thesis.

1.2: Motivation and previous studies

1.2.1: Motivation

This study has implications for both paleoenvironmental reconstruction (Clifton and Dingler, 1984) and maritime engineering (Bagnold, 1946).

Ripple signatures in lithified sediments have long been used to characterize paleoenvironments. The better we understand the processes which form these ripples, the more we can infer from our observations of these features in rocks.

Ripples formed on the sea floor affect wave-driven sediment transport, as well as the energy loss of the waves as they approach the shoreline. These factors play a large role in determining shoreline erosion and the stability of structures built in nearshore environments.

1.2.2: Previous work

Clifton and Dingler (1984) divided ripples into three categories: orbital, suborbital, and anorbital, based on the relationships between ripple wavelength, grain diameter, and orbital excursion. Plotting wavelengths at equilibrium against the ratio of

orbital excursion diameter, d, to median grain size, D, is a useful way to visualize this characterization (see Fig. 1.2). Orbital ripples have wavelengths that vary linearly with orbital excursion, with a λ/d ratio of approximately 0.65 for predicted equilibrium conditions (Clifton and Dingler, 1984). Orbital ripples occur within a d/D range of 1000 to 3000. The wavelengths of anorbital ripples are independent of orbital excursion and depend only on grain size. Anorbital ripples occur for d/D values exceeding 5000. Suborbital ripples occur for intermediate d/D values (between 3000-5000). The ripple wavelength of suborbital ripples appears to be some function of both the orbital diameter and grain size, but this relationship is not well defined (Clifton and Dingler, 1984). For this study, values of d/D are 2000 and 2400 for the 50 and 60 cm runs respectively, whereas the value for the 80 cm run is 3200. Thus, equilibrium ripples formed at the 50 and 60 cm excursions are expected to be the orbital type, while those at the 80 cm excursion should be sub-orbital.

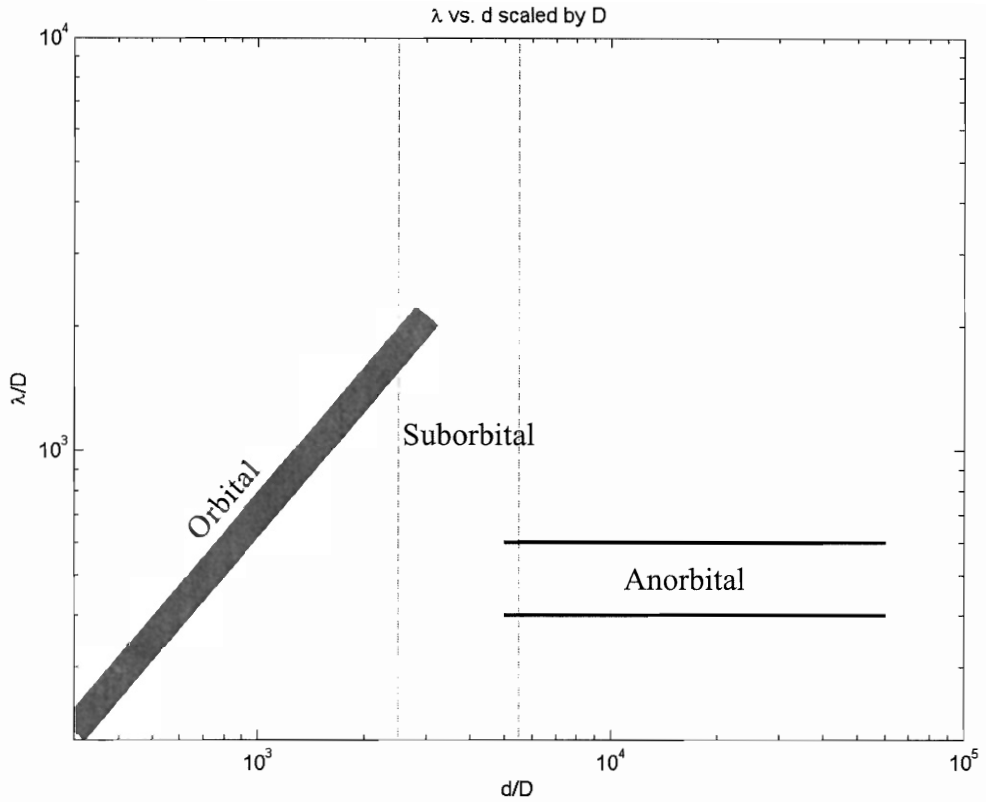

Figure 1.2: Schematic diagram showing the ranges of orbital, suborbital and anorbital ipples classified by the ratio of λ/D against d/D. After Clifton and Dingler (1984)

The principal studies of the temporal evolution of sand ripples to which I will compare my results are Lofquist (1978), and Davis *et al.* (2004).

Lofquist performed a series experiments in an oscillatory flow water tunnel in order to investigate the initiation of ripple development, growth of ripples, transitions of ripple states, and the attainment of equilibrium. Three sand sizes were used: D= 0.18 mm, 0.21 mm, and 0.55 mm. Twenty-four of his 104 experiments were initiated from a flatbed state. The wave period was reduced until the sand was mobilized, and that period was fixed for the duration of the experiment. He interpreted his results in terms of non-dimensional scaling of the time (by oscillation period and D/a ratio) and of the ripple wavelength and height (by λ/a and η/a).

Davis *et al.* (2004) used a 30 m long, 1.2 m wide, 0.9 m deep wave flume to study ripple growth and ripple transition. For ripple growth, the bed was studied as it evolved from a non-rippled to a rippled state. In ripple transition experiments the bed was studied as it evolved from one rippled state to another. The changes in bed state were caused by changes in surface wave conditions produced in the flume tank. Davis *et al.* (2004) were able to fit their ripple evolution observations to the logistic equation

$$\frac{dE}{dt} = \alpha E\left(E_f - E\right) \tag{1}$$

where E is the instantaneous energy level of the bed, E_f is the final energy level of the bed, t is the time in minutes, and α is the evolution rate constant. The general solution to equation (1), from Davis *et al.* (2004), is

$$E = \frac{E_f E_0}{E_0 + \left(E_f - E_0\right)e^{-\alpha E_f t}} \tag{2}$$

where E_0 is the initial energy level of the bed. From the fits to the logistic curve (2), the evolution rate was calculated. Davis *et al.* (2004) concluded that there was no difference between evolution rates obtained from the growth tests and those obtained from the transition tests.

Differences exist between this thesis, and those studies to which I am comparing my work. The most obvious difference is the experimental setup (see Chapter 2). Both Davis *et al.* (2004) and Lofquist (1978) use an apparatus in which the water moves in an oscillatory fashion relative to the sand bed. In my experimental design, a ripple cart is used to move the sand bed in an oscillatory fashion relative to the water. All of these approaches make an effort to mimic conditions observed in a coastal setting, but obvious

differences exist between the laboratory scenario and natural conditions. (e.g. space limitations, grain size differences, energy control, climate, biological effects).

My observational techniques are different from those of Davis *et al.* (2004), and Lofquist (1978). Lofquist (1978) relied on written observations, supplemented with photographs of the sand bed. Davis *et al.* (2004) used an Automated Sediment Interface Laser Scanner to make underwater scans of the sediment surface every 5 minutes. In my study there are three underwater cameras that capture video of the sand bed at given time intervals. I also make use of a digital camera to take calibrated pictures of the bed profile through the tank sidewall at various stages of its evolution.

2.0: Approach

2.1: Ripple cart

2.1.1: Theory

The ripple cart was constructed as a means to investigate sand ripple formation and development under oscillatory flow in a laboratory environment. The ripple cart was designed in such a way that conditions simulated in the laboratory are similar those encountered in nearshore marine environments. The cart can achieve orbital excursions up to 180 cm with a 10 s period, and creates a frictional boundary layer on the scale of 5-10 cm, which is consistent with field observations (Hay and Mudge, 2005, Miller and Komar, 1980b). In shallow water, wave height, H, wave period, T, and orbital excursion are related by the equation:

$$H = \sqrt{\frac{h}{g}}\frac{2\pi}{T}d \qquad (3)$$

(Kundu and Cohen, 2004), where h is the water depth, and g is the acceleration due to gravity. At a water depth of 10 m, typical of that in nearshore environments, equivalent wave heights for this experiment can be calculated using equation (3):

d = 50 cm: H = 32 cm

d = 60 cm: H = 38 cm

d = 80 cm: H = 51 cm

The similarities to nearshore conditions are what make the ripple cart a valuable tool in the study of sand ripples under oscillatory flow. Sand ripples, in natural nearshore conditions, are created by the back and forth motion of water over the sand bed at a wavelength proportional to the orbital excursion of the water near the bed. In the laboratory, the ripples are created by the back and forth motion of the bed relative to the water, with a wavelength proportional to the excursion of the cart. From the frame of reference of the sand particle, the two situations are the equivalent.

2.1.2: Design

The ripple cart (see Fig. 2.1) was designed by Dr. Alex Hay, and constructed during the past 1.5 years by Matthew Hatcher and Joseph Iuliucci starting as a summer project in 2005. The ripple cart was in working condition in January of 2007. Expense and space limitations were the primary reasons why the cart was designed so that the tray moves back and forth rather than the water.

The ripple cart facility consists of a mobile tray and stationary tank. The tank in which the tray is situated is 7 m long, by 1 m wide by 1 m deep. The sand rests on the tray, which is suspended from a wheeled cart on rails. The tray measures 1.83 m long by 0.78 m wide. Motion of the wheeled cart is achieved by an arm connected to a

synchronous motor drive. The motor turns the arm in a counterclockwise fashion, and this circular motion is converted to linear motion by a Scotch yoke mechanism. (See Fig. 2.1 and 2.2).

The position of the cart as a function of time is monitored by a range finder (Pasco motion sensor (PS-2130)), which bounces acoustic waves off a reflector attached to the cart (see Fig. 3.1j). The ranges are accurate to ± 1 mm, and are registered on a laptop computer.

Figure 2.1: Photograph of the ripple cart facility

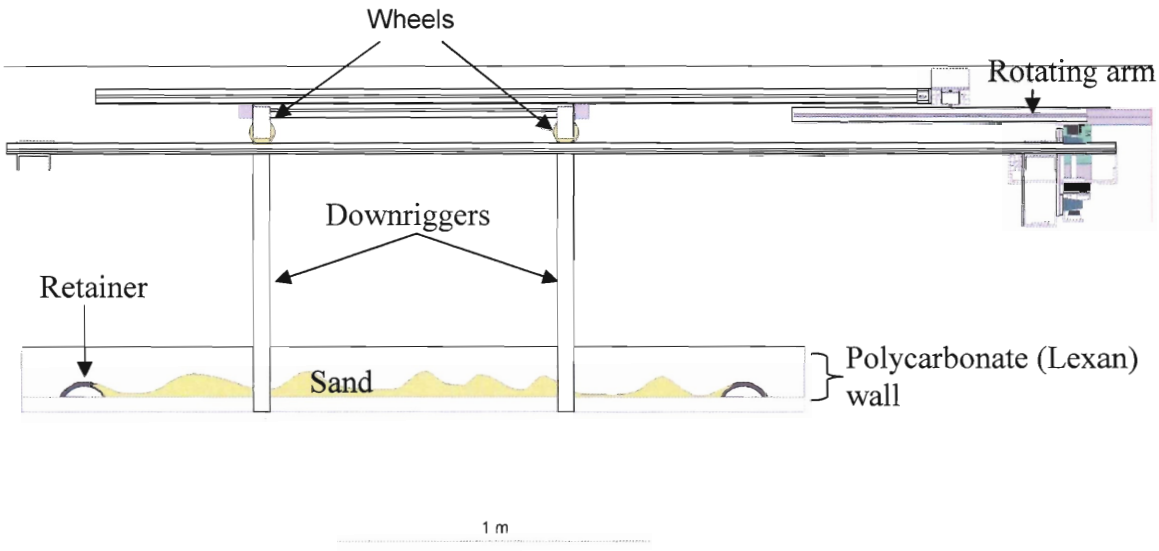

Figure 2.2a: Side-view scale drawing of the ripple cart (courtesy of Matthew Hatcher)

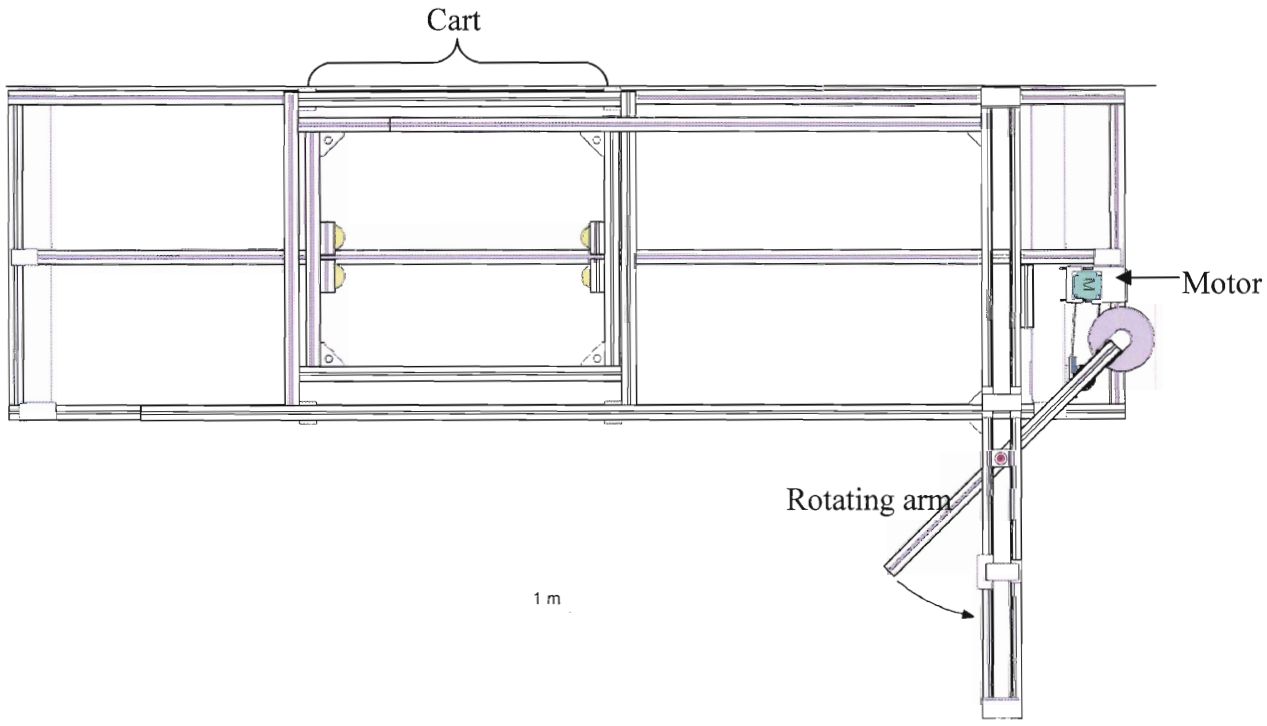

Figure 2.2b: Top-view scale drawing of the ripple cart (courtesy of Matthew Hatcher)

2.2: Experimental design

Three experiments were performed in the ripple cart facility, at excursions of 50 cm, 60 cm, and 80 cm. The period of the motion of the cart remained constant (10 s) for all three experiments. The orbital excursion of the cart can be adjusted by changing the position of the pivot on the rotational arm. Maximum velocity attained by the cart can be calculated from the formula:

$$v_{max} = \pi d/T \quad (4)$$

Values for v_{max} in this study are 15.7 cm/s, 18.8 cm/s, and 25.1 cm/s for the 50, 60 and 80 cm experiments respectively. Each experiment began in a non-rippled (flat bed) state. Flattening was achieved by a rectangular plate riding on the tray side walls. It was not possible to create a totally flat bed. The plate was dragged over the surface of the sand until the sand bed was 15 cm thick and the sediment surface was as smooth as possible. Examples of typical deviations from a flat surface resulting from the flattening process are shown in Figure 2.3.

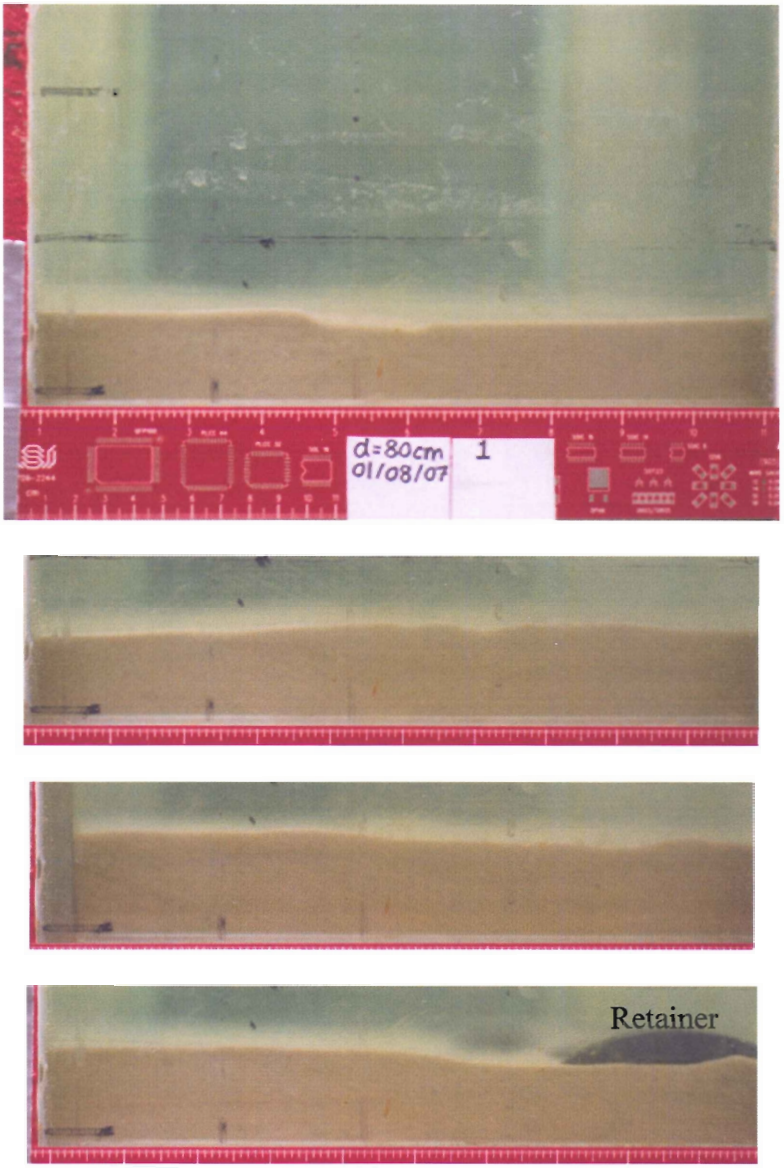

Figure 2.3: Examples of deviations from flat bed conditions produced by manual flattening of the bed surface. Photographs shown were taken before the start of the 80 cm experiment. The gradations on the ruler shown at the bottom of each photograph are at 1 inch and 1/10 inch intervals.

Every 15 or 30 minutes, depending on the rate at which the bed was changing, a set of three videos clips, one from each camera, was taken using the laser video system, and a set of photographs was taken using a digital camera. The videos were taken while the cart was in motion, and the photographs with the cart stationary. This process continued until the bed was thought to have reached equilibrium, which for the purpose of this experiment is defined as the point at which no further significant changes were observed in the bedforms.

2.3: Laser video system and camera

The bed topography during the experiments was recorded using a laser-video system (Crawford and Hay, 1998). The system consists of three underwater cameras and a laser which are hooked up to a Video Cassette Recorder (VCR) and screen, and connected to a capture device which records the video images on a computer at a rate of 30 frames per second. One camera is positioned at the end of the tank and records images along the length of the tray ("profile camera"). Another camera is located directly above the tray and provides a plan view of the bed surface ("down camera"). The third camera is at an angle to the bed surface, and provides a sidewards looking view along the bed ("left camera"). A laser is in place above the bed, and projects a thin light sheet onto the sediment, which is visible as the bright line in images obtained from the left camera. This beam, though not utilized in this thesis, will allow for accurate (mm) resolution of the bed surface when the camera calibrations have been completed. Figures 2.4a and 2.4b show the positions of the cameras, laser and range finder relative to the cart.

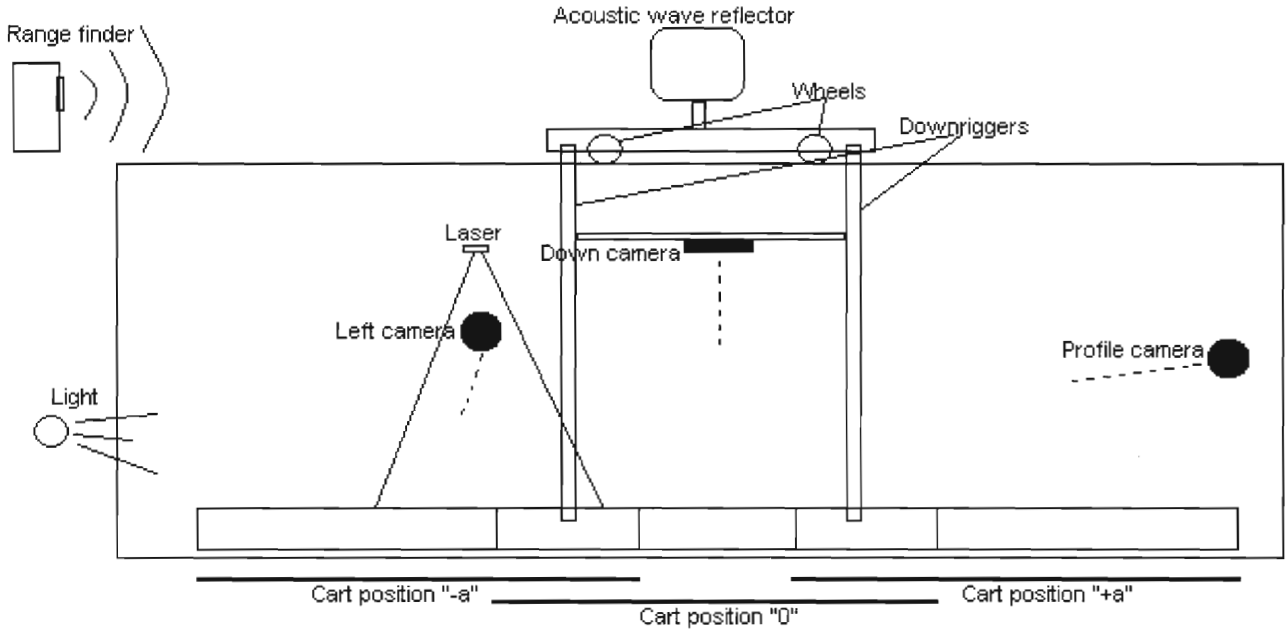

Figure 2.4a: Schematic diagram indicating the relationships between cameras, cart position, laser and light. Dashed lines indicate the direction in which the camera looks.

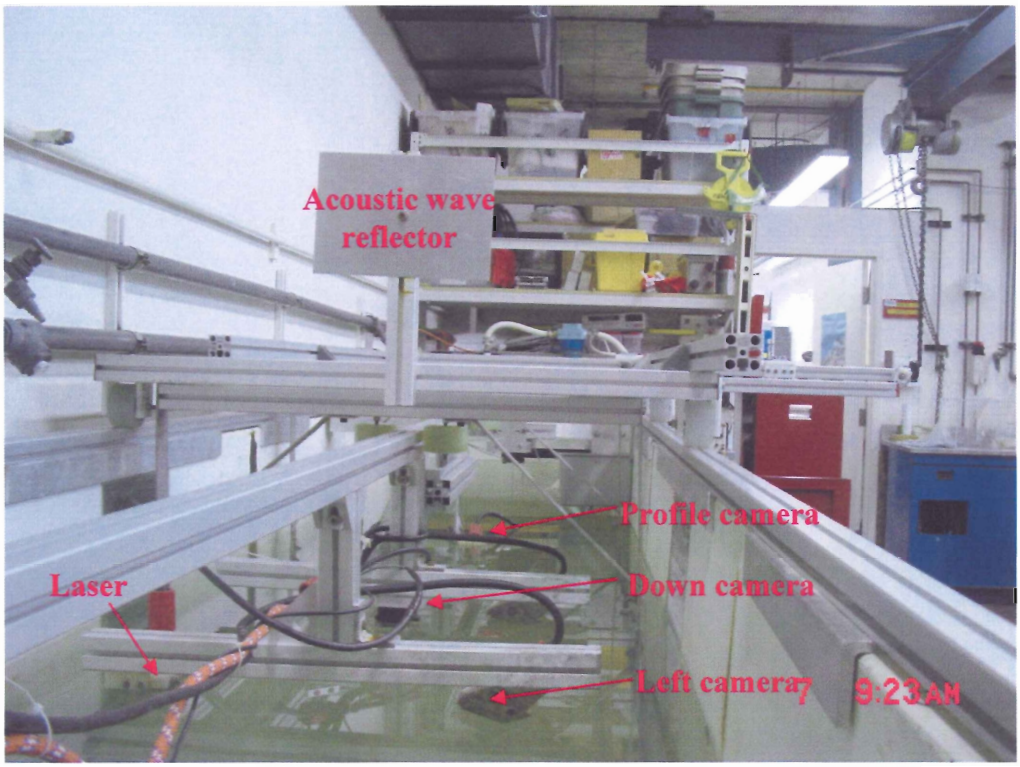

Figure 2.4b: Photograph of camera positions in tank.

A Nikon D80 SLR camera was used to take 10 Megapixel digital images through a 10 cm wide window of the side of the tank. These pictures, when overlapped, give a profile of the sediment surface along the full length of the tray. The distortion and magnification effects of the camera lens and tank window were investigated by taking photographs of a flat surface with a known grid pattern placed against the inside edge of the tray sidewall (i.e. in the same vertical plane as the sand-water interface in the photographs). The effects were found to be negligible.

2.4: Image processing:

After each set of video images was recorded, the motor drive was stopped. Pictures were taken of the bed profile through the tank side wall, at cart positions separated by 15 cm intervals in order to provide overlap of the images. Each set of pictures, when combined together, provides a profile of bed elevation along the length of the tray. Successive sets provide a record of the bed development over time. The images obtained from the NikonD80 were processed in stages using Matlab. First, the images were loaded into Matlab and cropped to exclude portions of the tank from the final image (an example of an uncropped image is presented in Fig. 2.3, top panel). The consecutive images were then stitched together. A piece of a ruler at the bottom of the image (see Fig. 2.3) provided a reference point for the stitching. The pictures were stacked along the reference point, and translated relative to this point according to their position along the tank, as given by the range finder and adjusted manually where necessary. Results of this process are presented in Section 3. The majority of the ripple profiles show light and darker coloured areas. The darker regions are where the sand is up against the

polycarbonate wall of the tray. The light regions represent the sand surface extending across the tank to the other side of the tray. Vertical exaggeration of the ripples in the resulting profile images (Section 3) varies from 5:1 to 12:1.

Obtaining the wavelength from the profiles was often somewhat subjective. Where it was clear, the dominant ripple crests were chosen. Where there was doubt, images of the entire bed obtained from the video cameras were employed to help determine the number of dominant peaks. This process was complicated by the fact that, in many cases, the sand against the fiberglass wall was the 2D expression of a 3D bedform. Wavelengths of the ripples were obtained by picking the coordinates of a sequence of dominant ripple peaks from the combined Matlab image of the bed profile. The difference of the positions of wave crests along the profile was averaged, which gave the approximate wavelength of the ripples. On average, 8 ± 4 peaks were measured to determine ripple wavelength (see Table 3.1). Figure 3.1i shows an example of picking ripple peaks.

2.5: Sand grain size determination

The sand used in these experiments was homogenous silica blasting sand, and has a median grain size of 250 μm (2.0 φ), which is typical of the sand grain sizes observed in nearshore environments.

Two methods of size determination were used: sieving and a settling column. The sieving was performed at Dalhousie University. Approximately 15 g of sample was used, and was shaken in a Ro-Tap for 15 minutes. The sand was sieved at quarter-phi intervals, ranging from 1.0 to 3.75 (Folk, 1980). The weight of the sand remaining on top of each

sieve was recorded, and these weights were used to produce a cumulative size distribution curve (Fig. 2.5).

In order to use the settling columns, which are located at the Bedford Institute of Oceanography (BIO), a sample size of approximately 1g was required. The sand is loaded in the top of the column, and allowed to settle to the bottom over a period of about 20 minutes. Once the particles reach the bottom of the column, they land on a dish which is attached to a sensitive scale. The settling column computer program uses Stokes' Law to calculate grain diameter (assuming spherical diameter of the sand particles).

$$\text{Stokes' Law: } V_s = \frac{2}{9}\frac{r^2 g(\rho_p - \rho_f)}{\nu}$$

where V_s is the settling velocity of the particle, r is the radius of the particle, ρ_p is the density of the particle, ρ_f is the density of the fluid, and ν is the fluid viscosity.

Whereas the sieving technique sorts grain size by the diameter of the sand particle, the settling column uses the settling rates of the particles in the sample to determine the size classes present. Table 2.1 and Figure 2.5 compare the results of both types of analysis. For calculations requiring median grain size, the numbers obtained from the settling column are used, since this method represents the dynamical aspects of sediment behavior in active transport conditions.

Table 2.1 Comparison of sieve and settling column results

Method	D_{16} (μm)	D_{50} (μm)	D_{84} (μm)
Sieve	330	230	150
Settling column	360	250	180

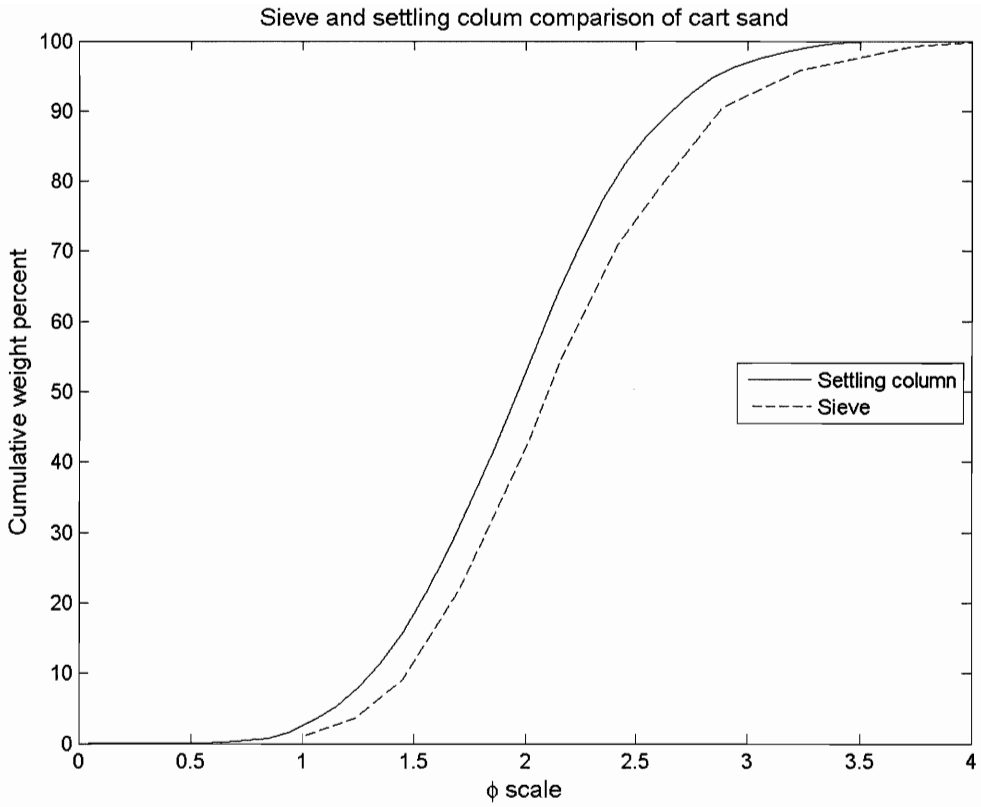

Figure 2.5: Cumulative size distribution curve of sand used in experiment, obtained from sieving (dashed line) and settling column (solid line).

3.0 Results

Table 3.1 summarizes the observed experimental results from each experiment. Calculated results are presented in Chapter 4. The remainder of this chapter discusses each experiment in more detail.

Table 3.1: Tabulated mean wavelengths of all three experiments

d (cm)	λ(mean) (cm)	Δλ(Standard deviation) (cm)	Peaks measured	Time (hr:min)
50	6.9	0.8	4	2:13
50	8.8	0.8	4	3:55
50	9.5	3.5	5	6:10
50	9.6	3.1	12	7:46
50	9.3	3.9	13	8:19
50	12.7	5.2	15	10:30
50	16.7	5.1	11	13:10
50	20.9	4.8	9	15:18
50	25.6	6.1	7	17:28
60	7.2	1.3	6	1:28
60	11.2	2.5	15	2:38
60	19.7	4.7	8	5:20
60	19.6	3.8	7	7:33
60	27.6	10.7	6	9:42
60	27.1	10.1	6	11:57
60	27.2	9.4	6	14:43
60	41.1	1.4	4	17:24
60	42.6	7.6	4	19:37
80	9.1	3.07	19	0:07
80	15	7.5	11	1:15
80	18	8.7	10	2:11
80	24.6	8.5	6	3:22
80	21.9	12	7	4:38
80	25.2	14.8	6	5:29
80	26.4	15.1	6	6:21
80	38.5	3.1	4	7:31
80	48.5	12.3	4	8:40

3.1: 50 cm orbital excursion

At the 50 cm excursion, the time taken for the bedforms to reach what was thought to be an equilibrium state was about 17.5 h. Because the bed state changed slowly, videos and photographs were taken at 30 minute intervals. All areas of the bed did not develop at a uniform rate. The first ripples appeared along the sides of the tray

after 52 minutes, and the entire bed was rippled after 7hr14min. During this experiment the ripples remained mostly 2D.

The initial wavelength of the ripples was 6.9 cm with a standard deviation of 0.83 cm. The wavelength at the end of the experiment was 25.6 cm with a standard deviation of 6.1 cm. Wavelengths during the middle of the experiment are displayed in Table 3.1. Bed profiles from the experiment are displayed in Figure 3.1a to 3.1i. Figures 3.1j and 3.1k show images captured from the laser video system.

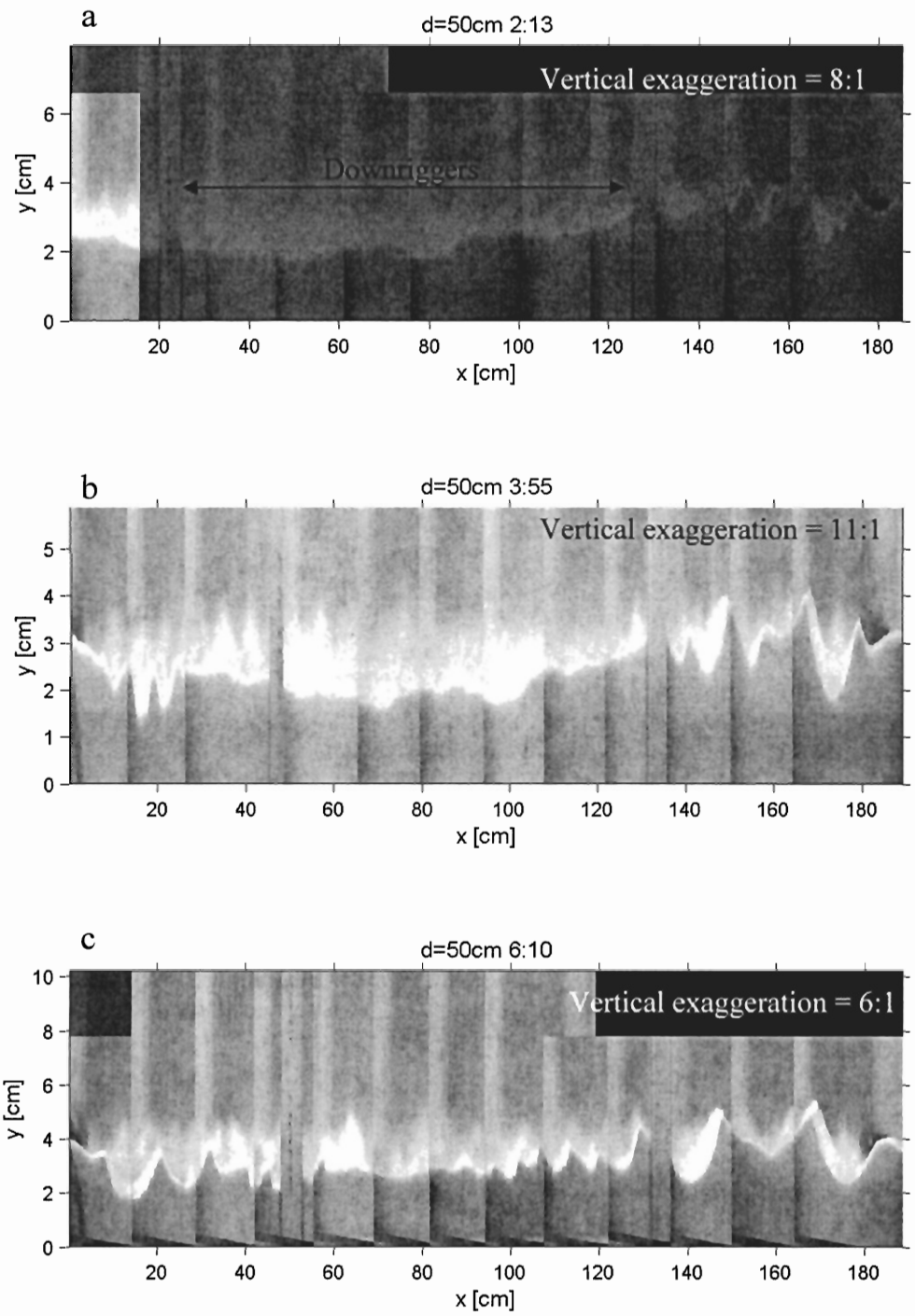

Figure 3.1a-c: Ripple profiles from d = 50 cm experiment.

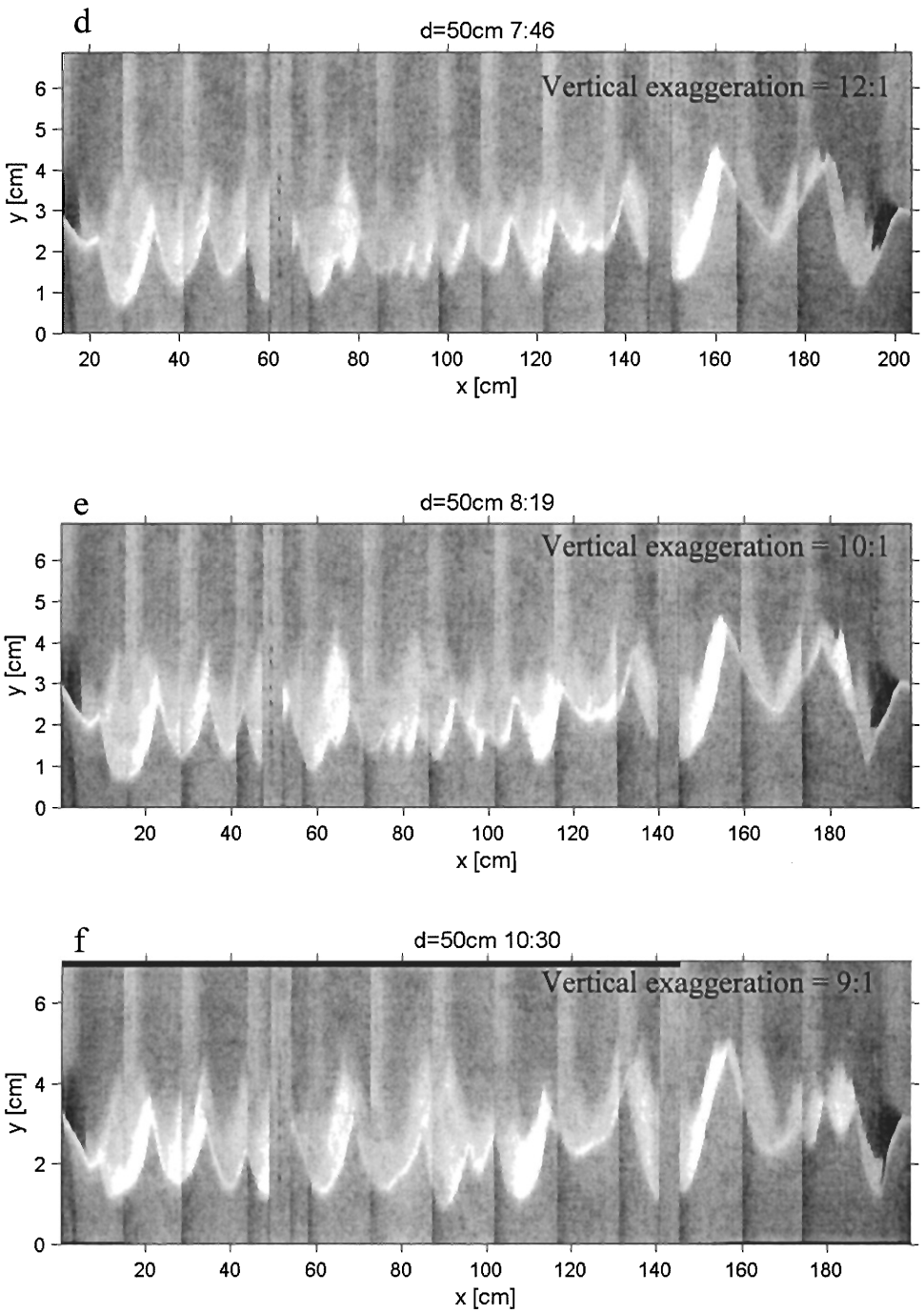

Figure 3.1d-f: Ripple profiles from d = 50 cm experiment.

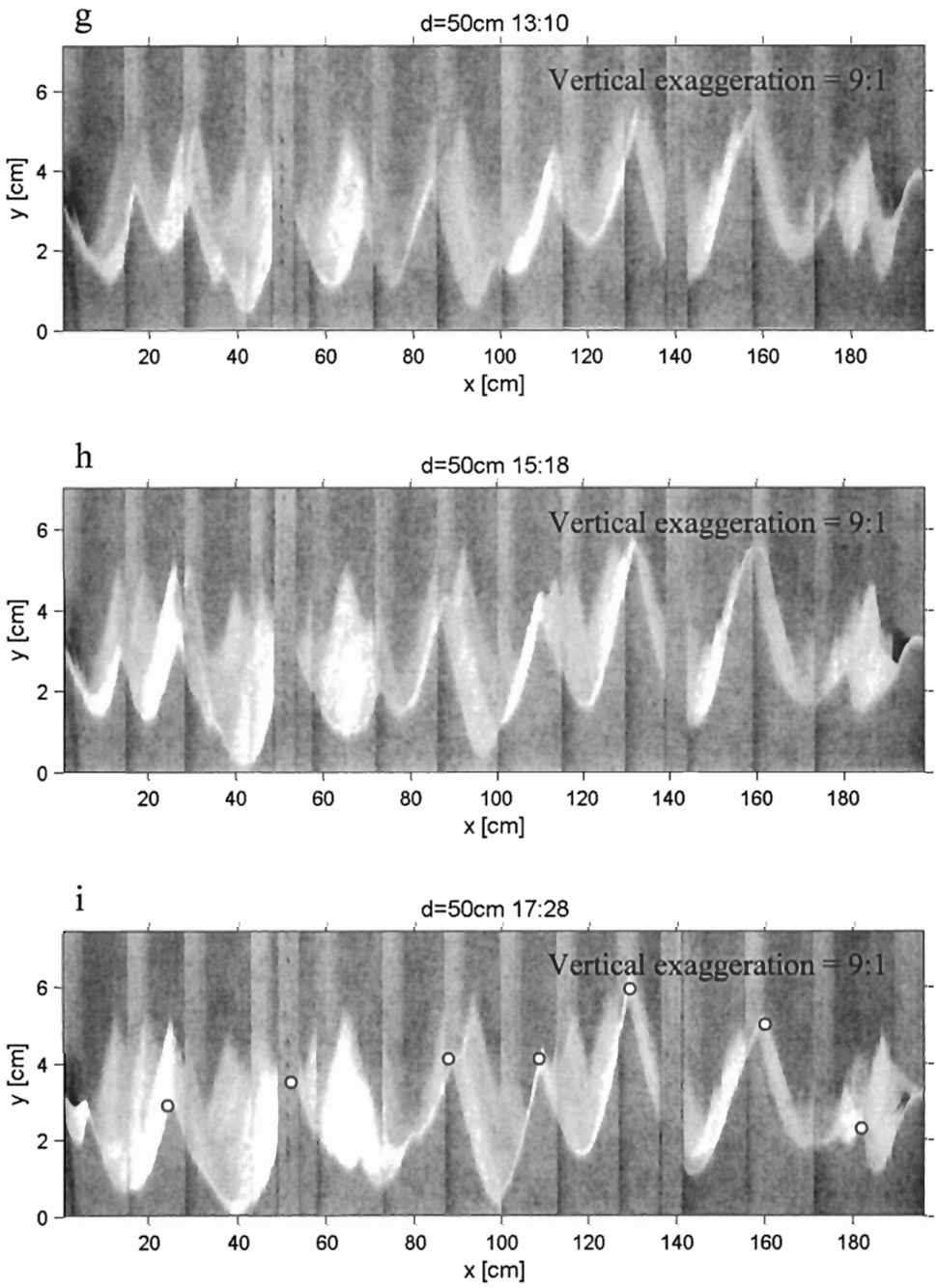

Figure 3.1g-i: Ripple profiles from d = 50 cm experiment. White circles in a represent ripple peaks used to calculate wavelength .

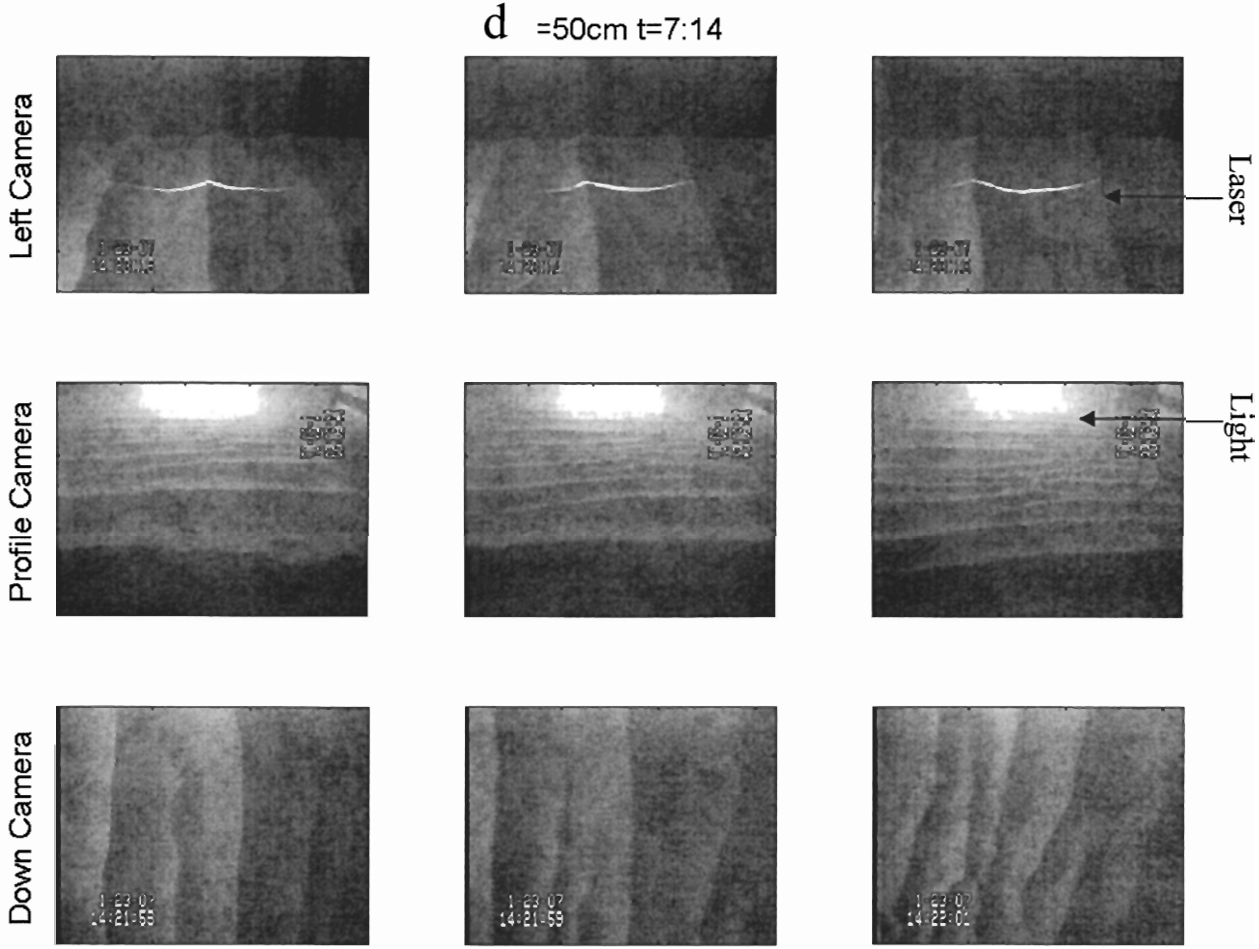

Figure 3.1j: Camera images from initial ripple development. The text in the corners of the images is the time stamp from the VCR. Left panels correspond to cart position "-a", centre panels to position "0", and right panels to position "+a". See Figure 2.5a and 2.5b. "Fuzziness" is a factor of the resolution of the VCR.

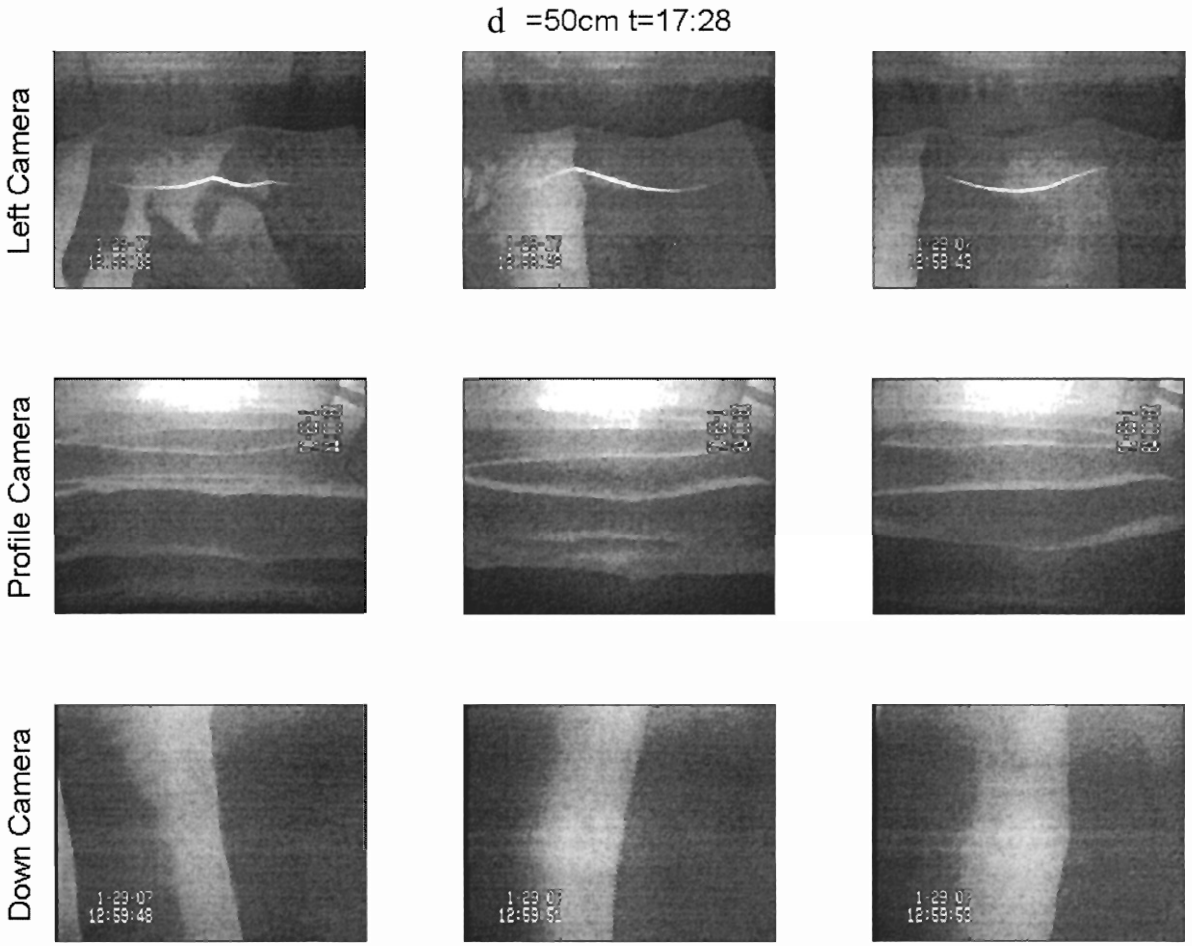

Figure 3.1k: Camera images from the end of the experiment

3.2: 60 cm orbital excursion

At the 60 cm excursion, the time taken for the bedforms to reach what was thought to be an equilibrium state was approximately 19.5h. For the first portion of the experiment, videos and photographs were taken at 15 minute intervals, and later at 30 minute intervals to accommodate the slowly changing bedforms. Again, areas of the bed did not develop at a uniform rate. The first ripples appeared along the sides of the tray after 17 minutes, and the entire bed was rippled after 1hr28min. The stitched images of the bed profile are presented in Figures 3.2a to 3.2i. Figures 3.2j and 3.2k show images captured from the laser video system. The wavelength of the initial ripples was 7.2 cm with a standard deviation of 1.3 cm. During the run, the ripples remained mostly 2D. The wavelength at the end of the run was 42.6 cm with a standard deviation of 7.6 cm.

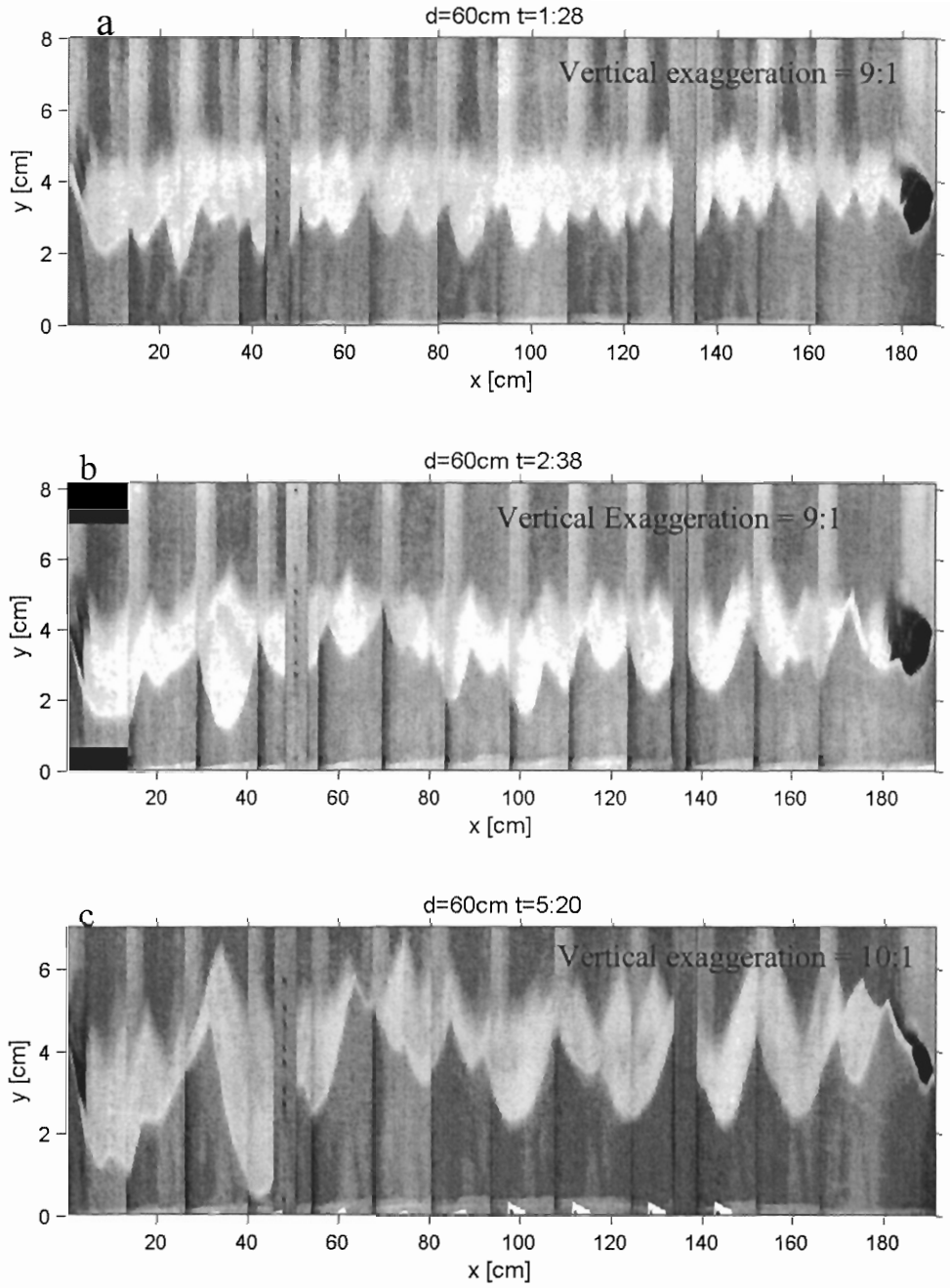

Figure 3.2a-c: Bed profiles from d = 60 cm experiment.

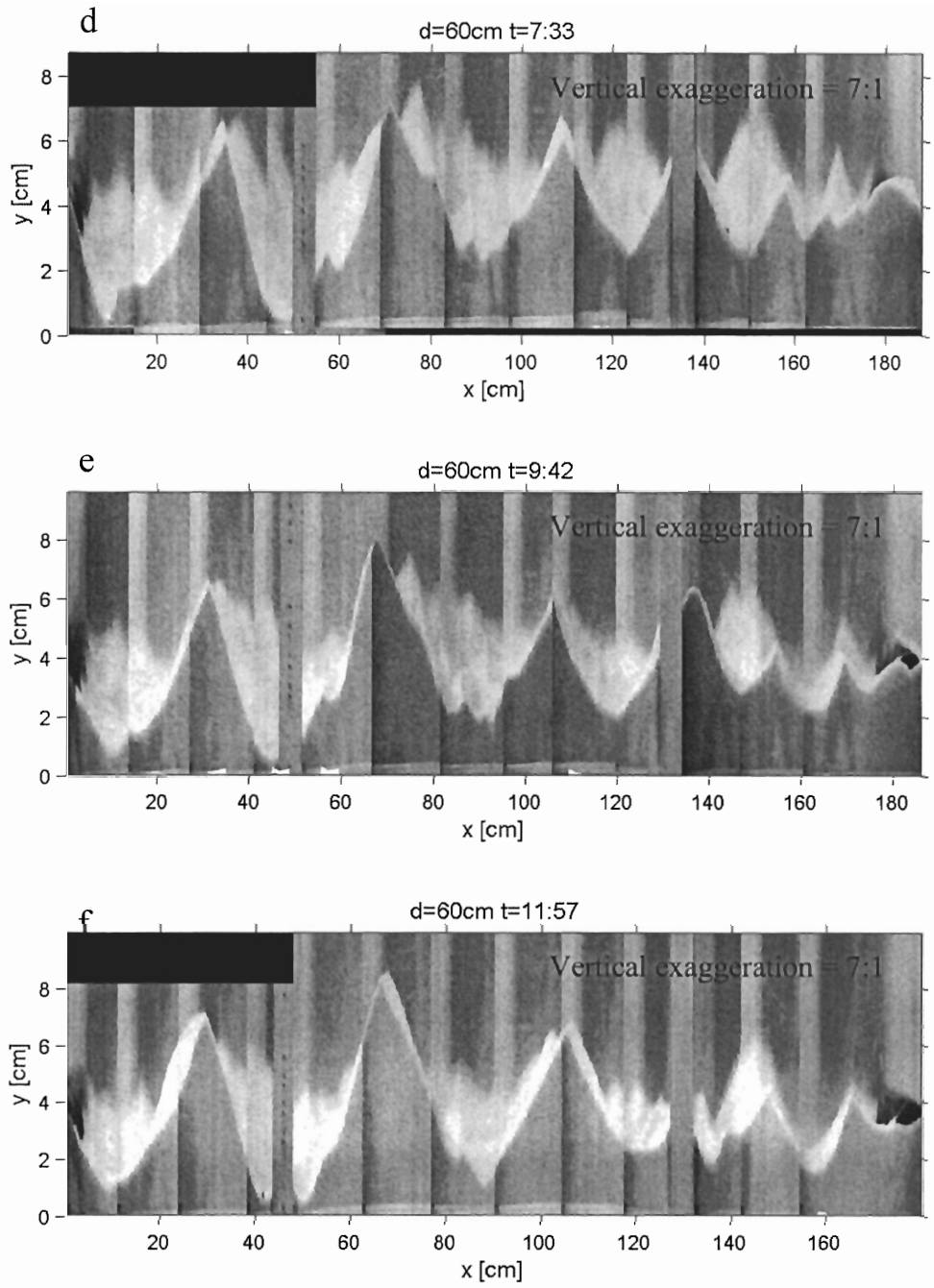

Figure 3.2d-f: Bed profiles from d = 60 cm experiment.

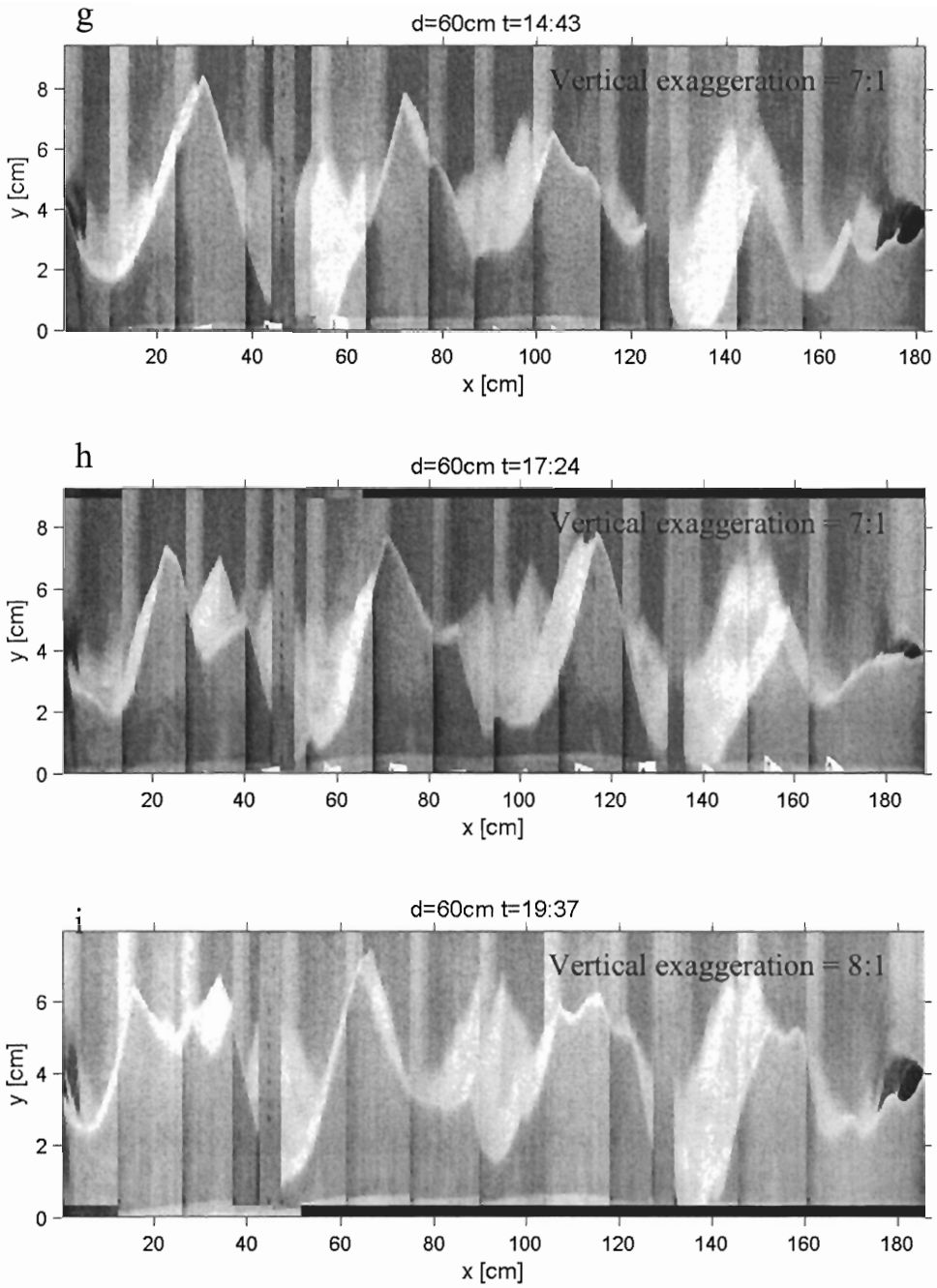

Figure 3.2g-i: Bed profiles from d = 60 cm experiment.

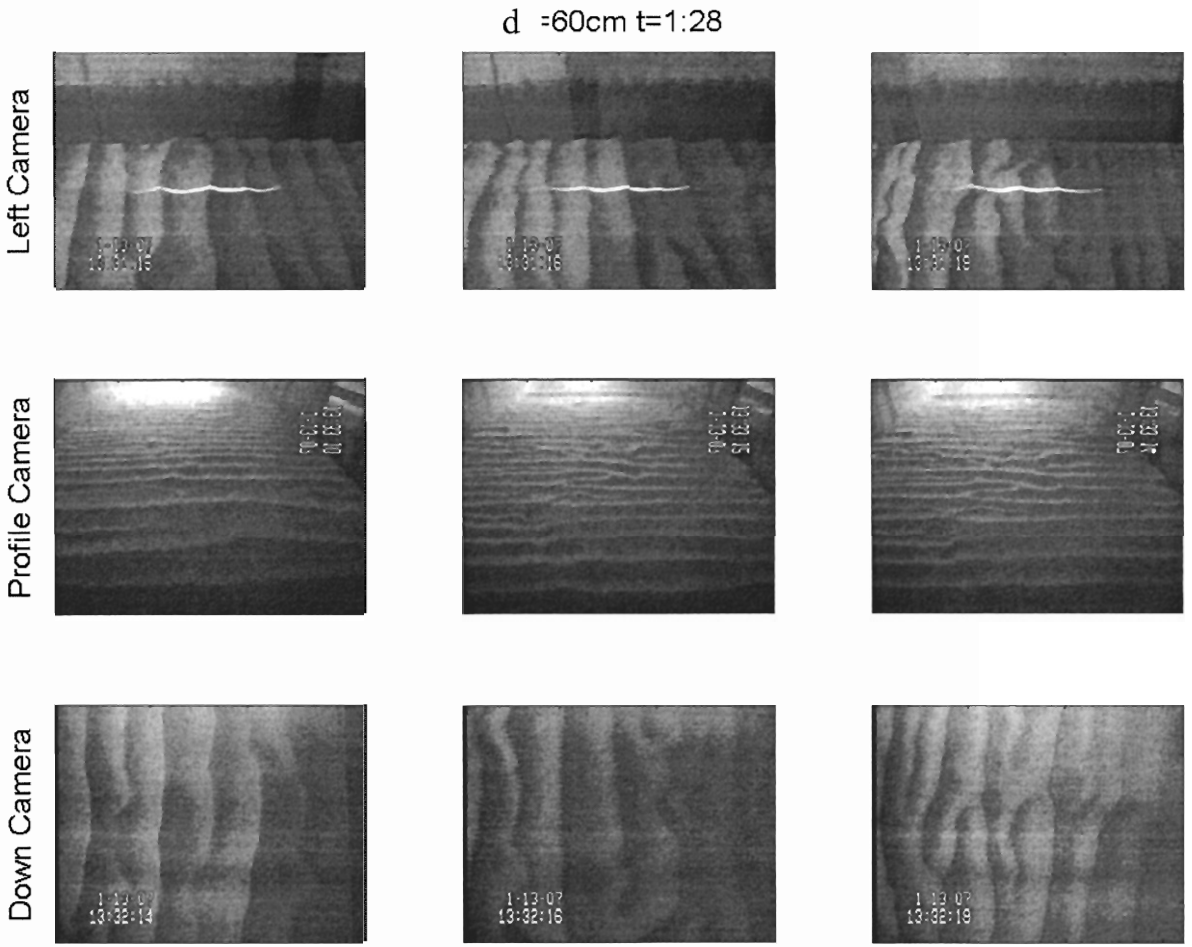

Figure 3.2j: Camera images from initial ripple development.

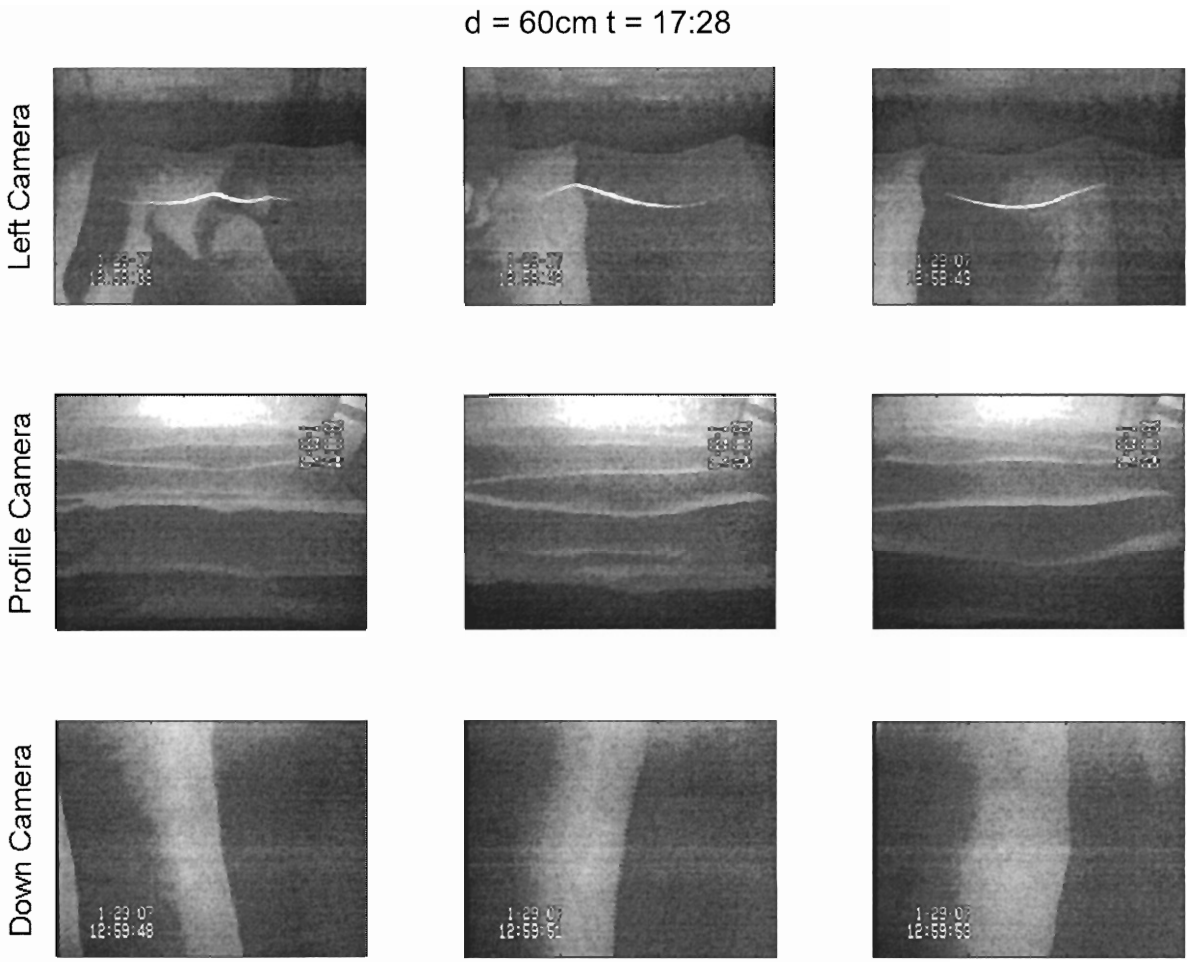

Figure 3.2k: Camera images from the end of the experiment.

3.3: 80 cm orbital excursion

At the 80 cm excursion, the time taken for the bedforms to reach what was thought to be an equilibrium state was about 8.5 h. For the duration of the experiment, videos and photographs were taken at 15 minute intervals due to the rapidly changing bed state. The entire bed was rippled in less than 5 minutes, the time at which the first set of videos was taken. The stitched images of the bed profiles are presented in Figure 3.3a to 3.3i. Figures 3.3j and 3.3k show images captured from the laser video system. The wavelength of the initial ripples was 9.1 cm with a standard deviation of 3.1 cm. During the run, the ripples achieved three dimensionality in approximately 40 minutes, and remained mostly 3D for the remainder of the run. The wavelength of the dominant ripples at the end of the run was 58.5 cm with a standard deviation of 12.3 cm.

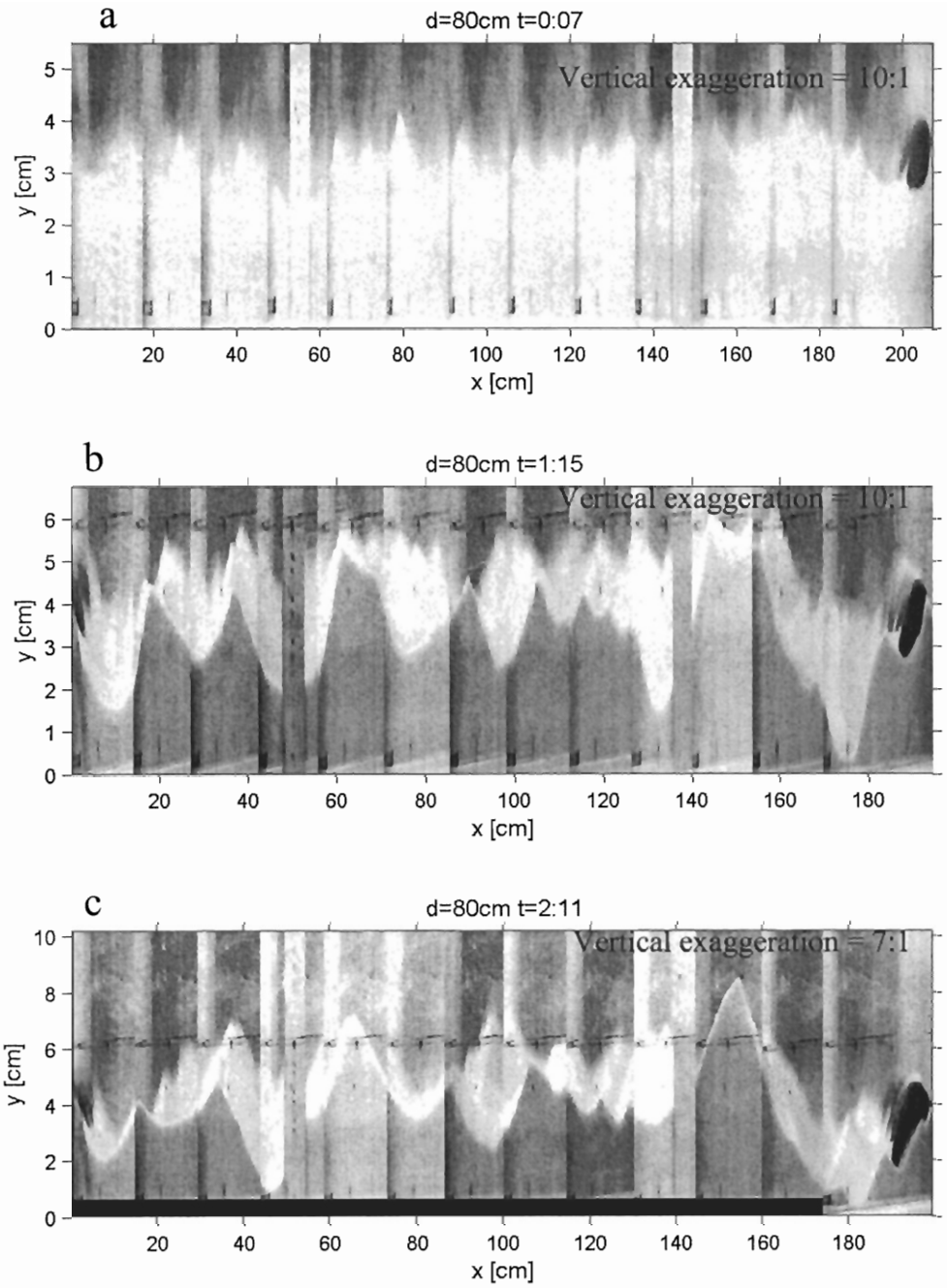

Figure 3.3a-c: Ripple profiles for the d = 80 cm experiment.

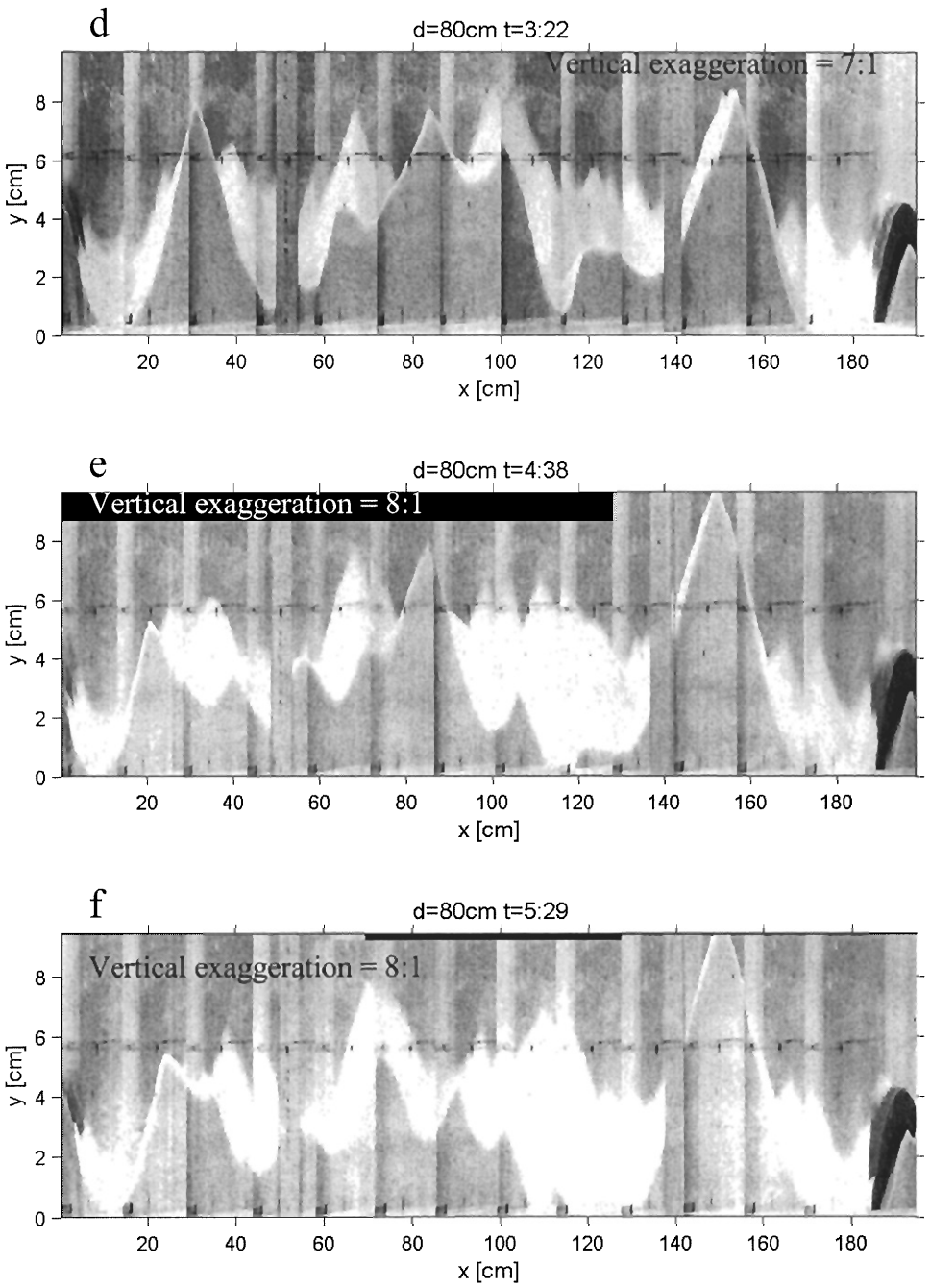

Figure 3.3d-f: Ripple profiles for the d = 80 cm experiment.

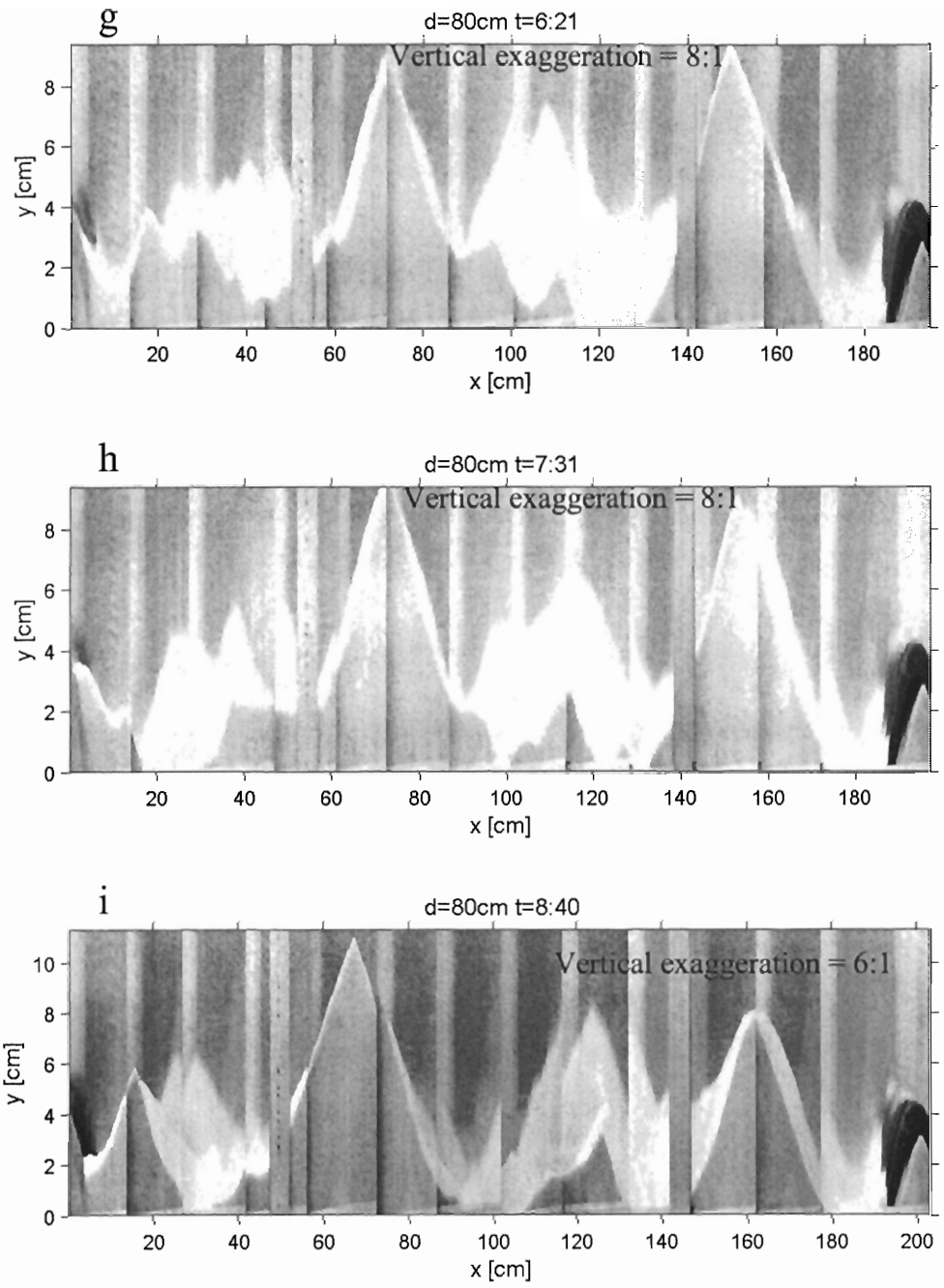

Figure 3.3g-i: Ripple profiles for the d = 80 cm experiment.

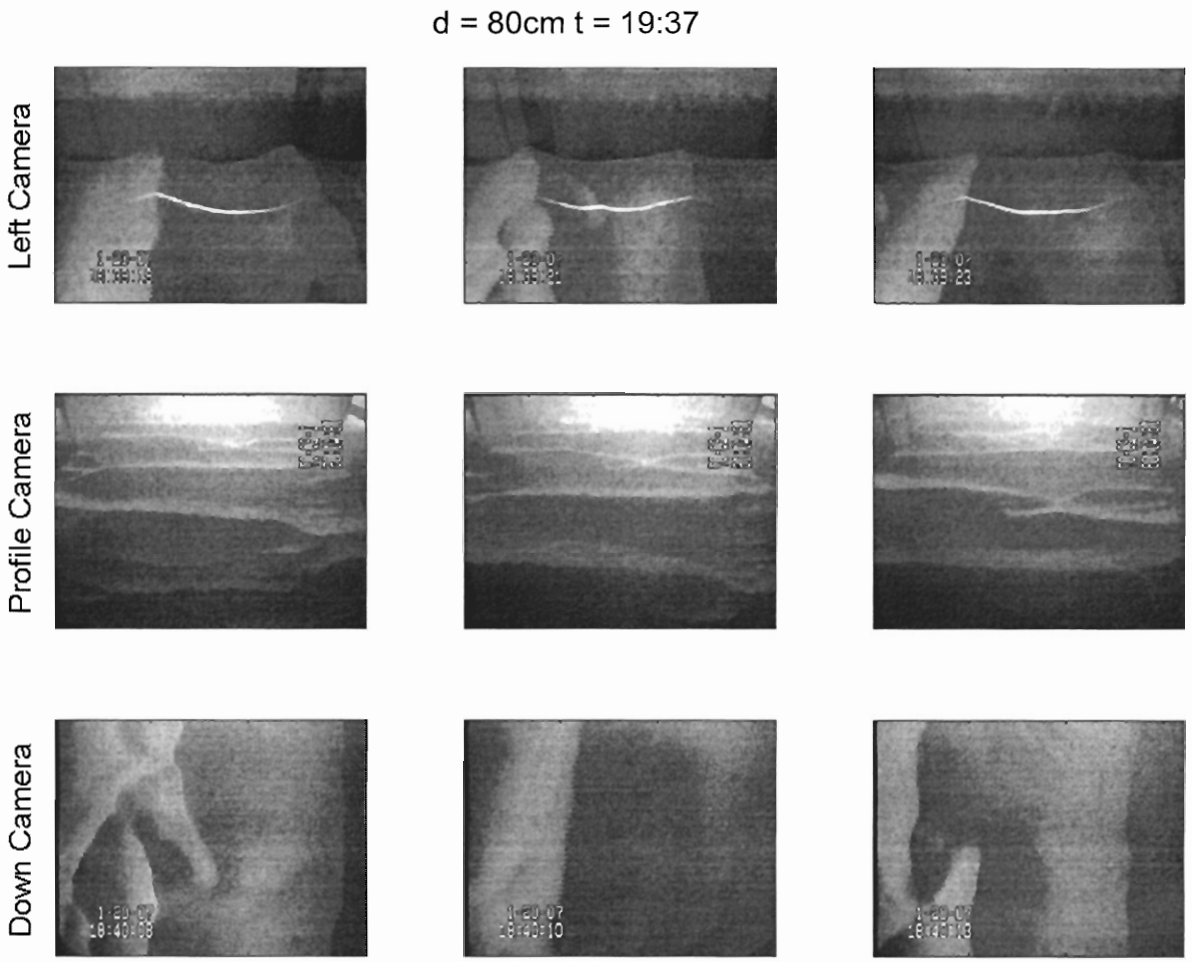

Figure 3.3k: Camera images from the end of the experiment.

4.0 Discussion

4.1: Qualitative description of growth and development of ripples

The ripple field in the d = 80 cm experiment developed rapidly and achieved a 3D state early on. This three-dimensionality was maintained throughout the duration of the experiment, with minor changes in the crest shape over time, making it difficult to tell when the experiment had reached an equilibrium state. The d=50 cm and 60 cm experiments developed in the same manner, but on different time scales. From the flatbed state, straight-crested ripples developed, and then merged to produce double spacing of the ripples, and the ripples increased in height. The ripple crests continued to split and reform, and the crest spacing continued to increase until no further significant changes were observed in the bedforms. Cross ripple-like features (smaller ripple sets within the troughs of the larger sets) occurred after approximately six hours during the 60 cm experiment, and also in the later stages of the 50 cm experiment, but did not persist. These cross-ripple occurrences are mentioned in passing, since they are not the focus of this thesis.

In all three cases, slight local elevations and depressions on the sand surface enhanced the formation of sand ripples in those locations (see Fig. 2.3). Ripples appeared first around these areas and along the sidewalls and ends of the bed, where there is a tendency for more grain motion to occur. It is my opinion that the initial conditions of the bed did not affect the final bed morphology in the three experiments.

4.2: Experimental value of λ/d

Miller and Komar (1980a) cite the relationship: $\lambda/d = 0.65$ for the predicted equilibrium wavelengths of orbital ripples. This relationship was obtained from all the data then available from wave flume, water tunnel, and oscillating bed experiments. Traykovski *et al.* (1999) observed a value of 0.74 for the ratio of ripple wavelength to orbital diameter using field data. Using experimental results of orbital diameter and wavelength, the observed values of this ratio can be calculated for the ripples in this study.

d=50cm: $\lambda_{observed}/d = 25.6/50 = 0.51$

d=60cm: $\lambda_{observed}/d = 42.6/60 = 0.71$

d=80cm: $\lambda_{observed}/d = 48.5/80 = 0.61$

Averaging these values gives $\lambda/d = 0.61$. This value is closer (6% difference) to that obtained by Miller and Komar (1980a) from laboratory data than to that of Traykovski *et al.* (1999) (19% difference) from field data. Figure 4.1 is a plot of λ/D versus d/D comparing the fit of experimental data to the calculated slope (this study) and the slope of Miller and Komar (1980a).

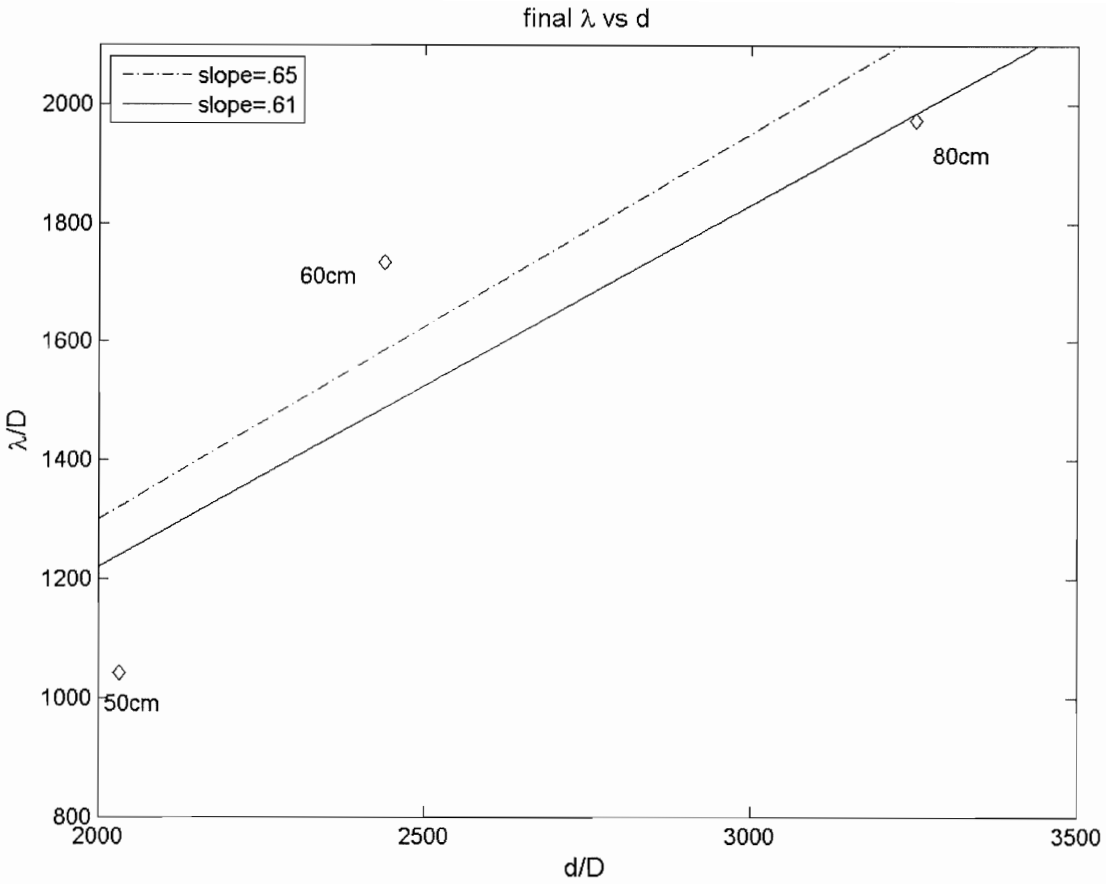

Figure 4.1: Relationship of final wavelengths to orbital excursions, scaled by D. Solid line is the slope calculated from experimental data. Dashed line is the slope calculated by Miller and Komar (1980a) from laboratory data.

4.3: Comparison to Lofquist (1978)

Lofquist (1978) plotted λ/a against (D/a)n, where n is the number of oscillation periods since the first ripples were observed, and where a is a measure of excursion that represents the excursion of the water relative to the fixed bed. This scaling collapsed Lofquist's data onto one curve. Lofquist drew an S-shaped curve (for which the equation was not specified) through his data points. This curve leveled off at approximately $(D/a)n \cong 1$. This result implies that ripple growth should be complete when $(D/a)n \cong 1$.

The following values of (D/a)n were calculated for the experiments, where a = d/2 and n is the total number of oscillations during each experiment.

50cm: (D/a)n = 6.0

60cm: (D/a)n = 5.8

80cm: (D/a)n = 1.9

Since (D/a)n is greater than 1 in each case, this scaling would imply that each experiment had run past the equilibrium point. Plotting experimental data on a graph with the same axes as Lofquist (1978), (see Fig. 4.2) yields quite a different result.

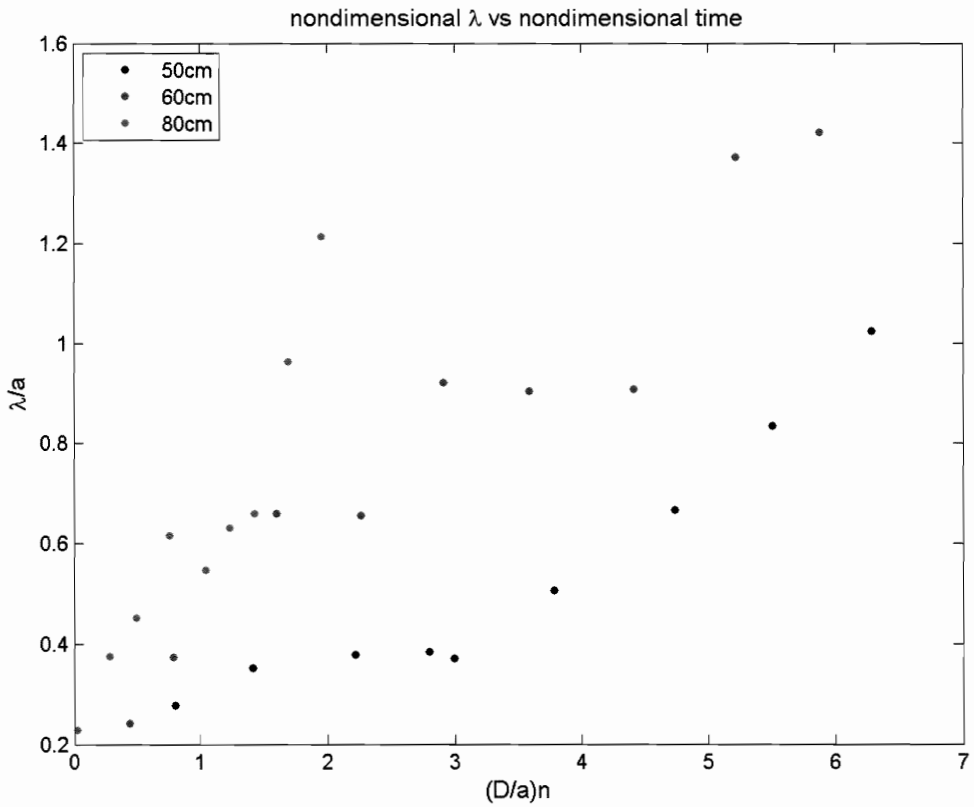

Figure 4.2: Experimental data non-dimensionalized using the scaling suggested by Lofquist (1978). This scaling does not collapse the data.

In Figure 4.2, we do not observe the same leveling off behavior of the ripples. The experimental data indicates that, although (D/a)n values greater than 1 were observed, the ripples had not yet reached equilibrium. The lack of agreement between the two studies can be attributed to the significant differences between the studies. The first issue with the comparison is in regards to the experimental design differences. Of the 20 experiments performed by Lofquist with D=0.21 mm sand (i.e. similar to that used in this study), only 4 were conducted beginning with a flat bed state. The parameters for these experiments are listed in Table 4.1. While the range of orbital excursions was comparable to this study, the maximum orbital velocities attained were, in general, much higher than those in this study because of the short oscillation periods. Maximum orbital velocities were calculated from equation (4).

Table 4.1: Orbital excursion, periods, and maximum velocities for D=218 μm sand from Lofquist (1978)

d (cm)	T (s)	v_{max} (cm/s)
36.6	4.01	28.7
27.4	3.33	25.8
55.0	4.59	37.6
73.2	6.02	38.2

In his plot of λ/a versus (D/a)n, Lofquist (1978) used measurements both from experiments with an initial flat bed and experiments beginning at a rippled state. This could contribute to the ripples in Lofquist's (1978) study reaching equilibrium at faster rates than those observed in this study. Another issue with comparing the two studies is the subjectivity of identifying the time at which ripples first appear. This problem was avoided in this study by using the time from which the cart began rather the time from which ripples first appear.

4.4 Comparison to Davis et al., (2004)

To quantify the temporal development of ripple wavelength, λ/a was plotted against time (see Fig. 4.3). Equation (5) represents the general solution of the logistic equation (1). The logistic growth law was proposed by Verhulst in 1838 as a means to describe the manner in which populations grow. The curve represents an initial stage of growth which is exponential in character, which levels off at a later time due to limiting factors within the population, such as competition. Fitting this curve to the data indicates that the ripples grew in a logistic manner.

$$\frac{\lambda(t)}{a} = \frac{1.5\frac{\lambda_0}{a}}{\frac{\lambda_0}{a} + (1.5 - \frac{\lambda_0}{a})e^{-\alpha 1.5t}} \tag{5}$$

where λ_0 is the initial ripple wavelength, α is growth rate, and $\lambda_f/a = 1.5$. The value of 1.5 was chosen to represent the approximate value of λ/a when ripple growth is complete and was derived from the relationship $\lambda = 0.75d$ (Traykovski *et al.*,1999). Calculating the R^2 values shows that this equation provides a reasonable fit to the data (see Fig. 4.3).

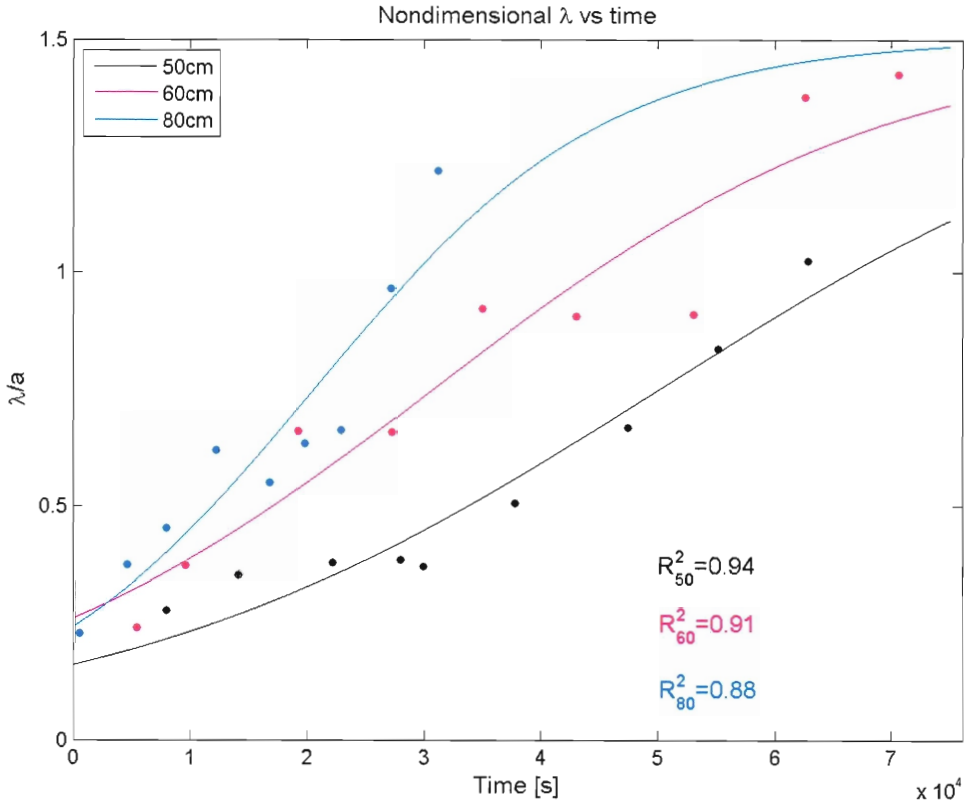

Figure 4.3: Non-dimensional wavelength versus time for d = 50, 60, and 80 cm.

From equation (5), ripple growth rates were determined for each experiment.

d = 50 cm, $\alpha = 0.28 \times 10^{-4}$ s^{-1}

d = 60 cm, $\alpha = 0.33 \times 10^{-4}$ s^{-1}

d = 80 cm, $\alpha = 0.53 \times 10^{-4}$ s^{-1}

The growth rates were used to non-dimensionalize the time axis, which had the effect of collapsing the data on to one curve (see Fig. 4.4). An R^2 value of 0.87 indicates that the logistic growth model is a good approximation of ripple growth during this experiment.

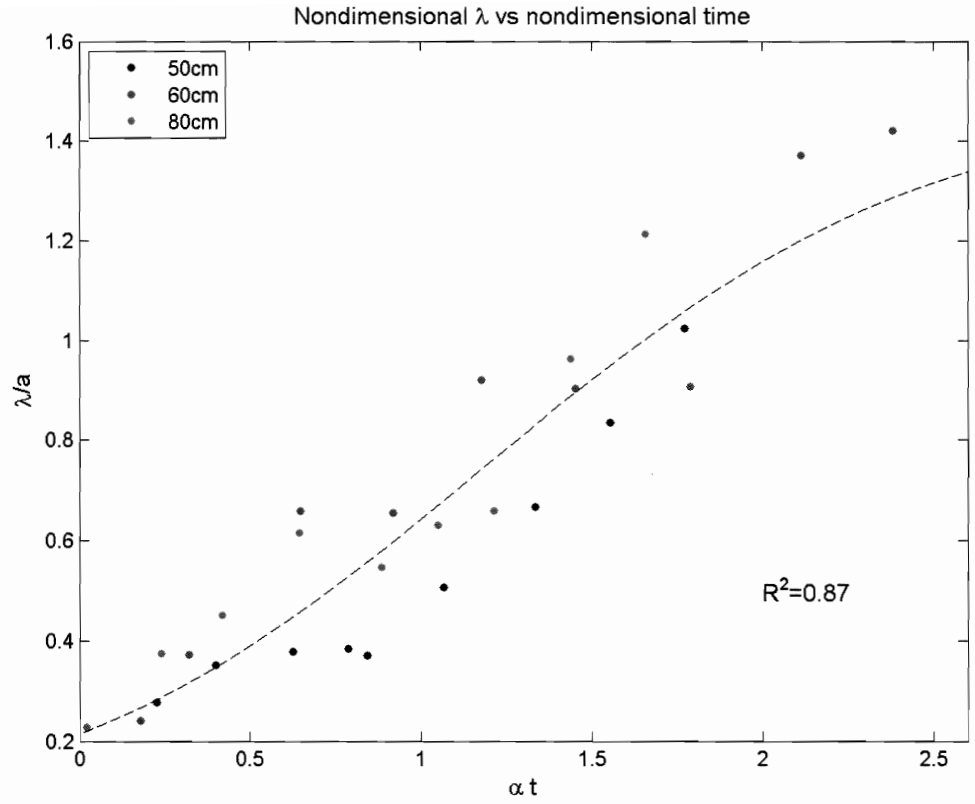

Figure 4.4: Non-dimensional ripple wavelength versus time non-dimensionalized by the logistic growth rate. Note that this scaling does collapse the data onto a single curve. Compare to Figure 4.2.

4.5 Conclusions

The development of a sediment-water interface of 250 μm median diameter sand from flat bed to a rippled state under orbital excursions of 50, 60, and 80 cm was observed at an oscillation period of 10 s. The bed evolved fastest at the 80 cm excursion, followed by the 60 cm excursion and then the 50 cm excursion (refer to Fig. 4.3). Both the 80 and 60 cm excursion experiments developed 3D bedforms during the experiment, with the 60 cm experiment returning to a mostly 2D state and the 80 cm experiment remaining mostly 3D. The principal bedforms observed, in order of abundance, were 2D and 3D ripples, and occasional cross ripples, which occurred at lower excursions. The

majority of the 2D ripples formed were orbital ripples. Suborbital ripples were also observed. The anorbital ripple range was not explored in this experiment. The experimentally derived wavelength to excursion relationship of $\lambda/d=0.61$ is comparable to other values reported in the literature (Miller and Komar, 1980a, Traykovski *et al.*, 1999).

The wavelength evolution through time was found to be well represented by a logistic growth curve, which, while consistent with the earlier findings of Davis *et al.* (2004), is nevertheless the first time that logistic growth of sand ripple wavelengths has been demonstrated for oscillation periods and excursions typical of field conditions. Davis *et al.* (2004) used water depths of 15-30 cm, wave periods between 0.83 and1.25 s and median grain sizes of 242 μm and 372 μm. Thus, while their sand size was comparable to typical beach sands, their water depth and wave period were much smaller than those usually encountered in coastal and nearshore environments during active transport conditions. The present experimental results were found to be inconsistent with the non-dimensional scaling used by Lofquist (1978).

I would expect that variations in the starting conditions of the bed (degree of flatness) would have significant effect on the initiation and initial development of the ripple bed. This was a factor in this experiment, since the bed flattening was done by hand, and did not produce a completely even surface at the start of each new run. This was observed especially during the 50 and 60 cm experiments, where ripples formed preferentially along pre-elevated sections. I do not believe that these starting conditions had a significant effect on the final wavelengths observed, because the memory of the initial conditions is lost by the time the bed is uniformly covered by ripples.

To follow up on these results, I would recommend that replicate experiments be performed to ensure that the results are reproducible. Experiments at different orbital excursions (a wider range than studied here) could also be useful in characterizing the bed development, as well as repeating these experiments with different grain sizes.

5.0 References

Bagnold, R.A. 1954. Motion of waves in shallow water: Interaction between waves and sand bottoms. Proceedings of the Royal Society of London, Series A (Mathematical and Physical Sciences) Vol **187** no 1008, pp 1-18.

Clifton, H.E and Dingler, J.R. 1984. Wave-formed structures and paleoenvironmental reconstruction. Marine Geology, **60**, pp 165-198

Crawford, A.M and Hay, A.E. 1998. A simple system for laser-illuminated video imaging of sediment suspension and bed topography. IEEE J. Oceanic. Eng. **23** (1), pp 12-19.

Davis, J.P., D.J. Walker, Townsend, M; Young, I.R. 2004. Wave-formed sediment ripples: Transient analysis of ripple spectral development, J. Geophys. Res., **109**, C07020

Folk, R. 1980. Petrology of sedimentary rocks. Hemphill Publishing Company. Austin, Texas. pp 31-32

Hay, A.E and Mudge, T. 2005. Principal bed states during SandyDuck97: Occurrence, spectral anisotropy, and the bed state storm cycle. J. Geophys. Res., **110**, C03013

Kundu, P and Cohen, I. 2004. Fluid mechanics: Third edition. Elsevier Academic Press. San Diego, California.

Lofquist, K. E.B. 1978. Sand ripple growth in an oscillatory-flow water tunnel. U.S. Army Corps Eng. Coastal Eng. Res. Center, Tech.. Paper No **78-5**

Miller, M. and Komar, P. 1980a. Oscillation sand ripples generated by laboratory apparatus. Journal of Sedimentary Petrology, Vol **50** No1 pp 173-182.

Miller,M. and Komar, P. 1980b. A field investigation of the relationship between oscillation ripple spacing and the near-bottom water orbital motions. Journal of Sedimentary Petrology, Vol **50**, No 1. pp 183-191.

Traykovski, P; Hay, A.E; Irish, J. D; Lynch J.F. Geometry, migration, and evolution of wave orbital ripples at LEO-15. 1999. J. Geophys. Res. **104** no C1. pp 1505-1524

Verhulst, P.F. 1838. Notice sur la loi que la population suit dans son accroissement. Corr. Math. Phys. **10** pp 113-121. See translation in Vogels, M. 1975. P. F. Verhulst's "Notice sur la loi que la populations suit dans son accroissement" from Correspondence Mathematique et Physique. Ghent, Vol. X, 1838. J. Biol. Phys. Vol **3** pp 183-192